

The Power-Oriented Graphs Modeling Technique

FROM THE FUNDAMENTAL PRINCIPLES TO THE SYSTEMATIC,
STEP-BY-STEP MODELING OF COMPLEX PHYSICAL SYSTEMS

DAVIDE TEBALDI*, and ROBERTO ZANASI

University of Modena and Reggio Emilia, Department of Engineering Enzo Ferrari, Via Pietro Vivarelli 10, Modena, 41125, Italy

* Corresponding Author

Email addresses: davide.tebaldi@unimore.it, roberto.zanasi@unimore.it

This work has been submitted to the IEEE for possible publication. Copyright may be transferred without notice, after which this version may no longer be accessible.

Understanding the physical laws governing physical systems has always been a subject of study for many world-renowned scientists throughout history. A significant contribution was given by James Clerk Maxwell [1], who elaborated on the relations between the mechanical motion of a medium and the observed phenomena of magnetism and electricity. The existence of a unified framework for the study of physical systems in different energetic domains started to become popular in the last century thanks to the work of Gabriel Kron, who showed that the modeling and simulation of mechanical and hydraulic systems can be effectively performed using analogous electrical systems based on tensor analysis [2]. It is from this unified framework that graphical modeling techniques such as Bond Graph (BG) [3], [4], Power-Oriented Graphs (POG) [5]–[7], and Energetic Macroscopic Representation (EMR) [8], [9] were first inspired and developed, and have subsequently evolved over the years. Independently of the chosen modeling approach,

comprehending the dynamics governing the evolution of the system trajectories is a first step for control engineers in order to develop suitable control laws for the considered system [10]. For this reason, the ability to develop compact models that accurately represent the dynamics of the systems under consideration is of great interest in the field of control and systems engineering [11]. Together with the graphical modeling techniques POG, BG, and EMR, the modeling of physical systems can be addressed using a variety of approaches and methodologies available in the literature, where the chosen approach typically depends on the energetic domain of the system under consideration.

Historically, one of the most well-known approaches for modeling mechanical systems has been the Lagrangian approach [12], [13]. Among the areas of application of this approach, robotics stands out, since the Lagrangian equations are used to derive the classical robot manipulator dynamics [14]. This applies to many different types of robotic manipulators; for instance, in [15], the Lagrangian equations are used to derive the dynamics of wheeled mobile robots. Another area of application is represented by vehicle dy-

Digital Object Identifier 10.1109/MCS.2020.000000

Date of current version: XXXXXX

namics. As an example, a comparison between Lagrangian mechanics and the POG technique when modeling a full toroidal variator [16] is given in [17]. Depending on the specific mechanical system under consideration, the Lagrangian approach may be replaced by other approaches, as in [18], where vehicle differentials are modeled using a set of algebraic equations, in [19], where planetary gear sets are modeled using the Lever Analogy, and in [16], where full toroidal variators are modeled using a Newtonian approach.

As far as the electrical and electromechanical domains are concerned, reference can be made to power converters [20] and to Permanent Magnet Synchronous Motors (PMSMs) [21], which are used in applications such as power grids [22] and hybrid or plug-in electric vehicles [23]–[25]. Power converters are typically modeled in the form of equations [26], [27] and can be simulated using dedicated platforms such as the Piecewise Linear Electrical Circuit Simulation (PLECS) simulator [28]. Permanent magnet synchronous motors are typically modeled in the form of equations by giving the system equations in the d-q reference frame [29], [30] or in the static reference frame [31], [32].

The modeling problem becomes more complex when physical systems composed of elements belonging to different energetic domains need to be addressed. Devices such as Electro Continuously Variable Transmission (ECVT) [33], [34] or hydraulic CVT [35], [36], which can be found in hybrid vehicles, include physical elements in the electromechanical and hydromechanical domains, respectively. Mechatronic machines [37], [38] generally include physical elements in different energetic domains interacting with each other, and the same observation applies to robotic systems as well, which nowadays find applications in many fields including manufacturing, medical, and social sectors [39]. Many other examples of multi-physics systems [40], composed of physical elements from various energetic domains, can be found. This is because engineering applications typically involve the interaction of different physical systems. In these cases, it can be more appropriate to use port-based modeling approaches [40]. The main dedicated graphical modeling techniques which are suitable for modeling physical systems in different energetic domains are the aforementioned POG, BG, and EMR. These techniques have been widely employed in a range of applications over the years for the study of multi-physics systems. They are based on the same unified concepts of energy and power, but offer different pros and cons relative to each other [41]. In this article, we dedicate a sidebar to comparing POG, BG and EMR, with reference to an example used as a case study, as shown in “Comparison With Other Graphical Modeling Techniques”. Graphical modeling techniques introduce a unified modeling framework [42] which, unlike purely analytical tools, also offers effective and energy-based graphical descriptions of physical systems.

At the beginning of its history [3], BG was mainly applied to the modeling of mechanical systems [43], while variants of BG were proposed in order to model systems such as transmission lines [44].

Summary

Modeling physical systems is an essential skill for a control engineer, since it enables to achieve a deep understanding of their dynamic behavior and, consequently, the development of effective control strategies. The first part of this article provides a tutorial description of the fundamental principles and properties of the Power-Oriented Graphs (POG) modeling technique. Various case studies in different energetic domains are then presented to consolidate the fundamental principles, each highlighting different features of the POG modeling technique. The latter is then compared with the other two main graphical modeling techniques available in the literature, namely Bond Graph (BG) and Energetic Macroscopic Representation (EMR). The second part of this article assumes once again a tutorial nature, in order to introduce the new Fast Modeling POG (FMPOG) procedure. The FMPOG, which operates in the POG framework, is a methodical step-by-step procedure that enables the readers to quickly derive the power-oriented graphical model of physical systems starting from their schematics. From the power-oriented graphical model, the state-space model can then be directly determined. To ensure the FMPOG procedure is easily usable by the entire community, we apply it to three examples in different energetic domains in this article, guiding the reader step-by-step through the derivation of the physical systems models.

BG has also found academic applications to provide students with a graphical tool for modeling systems in different energetic domains, such as the dynamics of a sink or simple electrical networks [45]. Later, BG was applied to electrical machines and power engineering [46], as well as to magnetic circuits [47] and hydraulic systems [48]. Nowadays, BG is also used with interconnections [49], in order to model multi-physics systems such as vehicle dynamics [50], robotic systems [51] or even biomolecular systems [52]. In the 90s, POG came into play [5]. Over the years, it has been employed for modeling a large variety of physical systems providing a valid alternative to BG thanks to the more intuitive graphical construction. Among the multi-physics systems modeled using the POG technique are automotive systems [17], [35], electrohydraulic systems [6], electrical machines such as PMSMs [21], power converters [20], and hybrid electric vehicles [34], [53], showing the versatility of the POG technique. EMR was lastly invented at the beginning of this millennium [8]. It adopts a different symbolism with respect to BG and POG, and can be employed for the modeling of multi-physics systems

Graphical modeling techniques introduce a unified modeling framework which, unlike purely analytical tools, also offers effective and energy-based graphical descriptions of physical systems.

as well, although they have been mostly employed for electromechanical systems such as electric machines [54], planetary gear sets [55] or entire hybrid electric vehicles [56].

In this article, we propose a new Fast Modeling Power-Oriented Graphs (FMPOG) step-by-step modeling procedure in the framework of the POG technique. The latter offers all the functionalities of the standard POG technique, including its applicability to different physical systems in different energetic domains. Additionally, FMPOG has the functionality of being methodical, since it consists in the application of a series of well-defined modeling rules following a step-by-step guided procedure.

The fundamental concepts of the POG technique are first described in this article, by also providing several modeling case studies of different complexity. These case studies are designed to cover all the main advantages of the POG technique, which include POG block schemes directly implementable in the Simulink environment, the functionality of reading the POG state-space model directly from the POG block scheme, and the potential to apply the so-called congruent transformations for model reduction. The mathematical model calculation is a functionality that simulators do not generally provide: the user can simulate the system schematic, which is typically obtained by dragging and connecting the different physical elements together, but this does not provide the user with the system dynamic model/equations. For simple systems, the state-space equations may be read from the schematic; however, as the number of physical elements increases, reading the state-space equations directly from the schematic may become very complex and easily subject to mistakes. Nevertheless, having the system dynamic model is highly desired, since it enables a control engineer to develop a proper control strategy for the system under consideration. Furthermore, the direct attainment of the state-space model starting from the graphical model is a functionality of the POG technique that is not available for the BG and EMR techniques. In this article, the new FMPOG procedure is proposed and applied to three examples in different energetic domains. We provide the general rules and the step-by-step procedure to be followed by the readers interested in modeling multi-physics systems.

FUNDAMENTALS

The POG is a graphical modeling technique adopting an energetic approach. Physical systems are modeled using a modular structure based on two main blocks: Elaboration Blocks (EBs), modeling dynamic and static elements, and Connection Blocks (CBs), modeling energy conversions. The main concepts which are employed are those of energy and power variables, whose description in the different energetic domains is given in the Section “Energetic Domains and Physical Elements” together with the description of the different physical elements. The elaboration and the connection blocks interact with each other and with the external world through the system energetic ports, also called power sections, as described in the Section “Modular Structure of the POG”. Depending on the type of connection characterizing the Physical Elements (PEs), which can either be of the series or parallel type, a proper generalization of the Kirchhoff’s laws can be applied, as further discussed in the Section “Series and Parallel Connections”. By combining together elaboration and connection blocks, the so-called POG block scheme is obtained. Once the POG block scheme is build, it is always possible to determine the so-called POG state-space model in the linear case [57], as illustrated in Section “POG State-Space Model”. One of the most appealing features of such POG state-space model, as opposed to the classical POG state-space representation, is its suitability for the application of state-space transformation for model reduction, as further discussed in Section “Congruent State-Space Transformations and Model Reduction”.

Energetic Domains and Physical Elements

When modeling physical systems, the main energetic domains are the electrical domain, the mechanical translational domain, the mechanical rotational domain, and the hydraulic domain, as enlisted in Table 1. Each energetic domain is characterized by three different types of physical elements: two dynamic elements D_e and D_f , storing the energy in the system, and a static element \mathcal{R} , dissipating the energy.

As an example, the sidebar “First Case Study: A DC Motor Driving an Hydraulic Pump” involves physical elements in three different energetic domains, that are electrical, mechanical rotational and hydraulic. Each energetic

The POG is a graphical modeling technique adopting an energetic approach. Physical systems are modeled using a modular structure based on two main blocks: Elaboration Blocks, modeling dynamic and static elements, and Connection Blocks, modeling energy conversions.

TABLE 1 The dynamic elements D_e and D_f , the static element R , the energy variables q_e and q_f , and the power variables v_e and v_f in the electrical, mechanical translational, mechanical rotational, and hydraulic energetic domains.

	Electrical	Mechanical Translational	Mechanical Rotational	Hydraulic
D_e	Capacitor C	Mass M	Inertia J	Hydraulic Capacitor C_I
q_e	Charge Q	Momentum p	Angular Momentum p	Volume V
v_e	Voltage V	Speed v	Angular Speed ω	Pressure P
D_f	Inductor L	Spring E	Rotational Spring E_r	Hydraulic Inductor L_I
q_f	Flux ϕ	Displacement x	Angular Displacement θ	Hydraulic Flux ϕ_I
v_f	Current I	Force F	Torque τ	Volume Flow Rate Q
R	Resistor R	Friction b	Angular Friction d	Hydraulic Resistor R_I

domain is also characterized by four different types of variables: two *energy variables* q_e and q_f , which are used to define the amount of energy stored within the dynamic elements, and two *power variables* v_e and v_f , which are used to define the energy movement within the system. The power variables v_e in Table 1 are called *across* power variables because they are defined between two points of the space, as shown in Figure 3: these variables coincide with the *effort* power variables defined in the BG technique as far as the electrical and hydraulic domains are concerned, and with the *flow* power variables defined in the BG technique as far as the mechanical translational and rotational domains are concerned [4]. The power variables v_f in Table 1 are called *through* power variables because they are defined at each point of the space, as shown in Figure 3: these variables coincide with the *flow* power variables defined in the BG technique as far as the electrical and hydraulic domains are concerned, and with the *effort* power variables defined in the BG technique as far as the mechanical translational and rotational domains are concerned [4].

The dynamic elements D_e are called *across elements* as they produce an across variable v_e as output power variable. At the same time, the dynamic elements D_f are *through elements* as they produce a through variable v_f as output power variable. The dynamic elements D_e and D_f , and the static elements \mathcal{R} , are characterized by two terminals, each of which characterized by a pair of power variables (v_{e1}, v_{f1}) and (v_{e2}, v_{f2}) , as shown in Figure 4(a). By defining $v_e = v_{e1} - v_{e2}$ and $v_f = v_{f1} = v_{f2}$ as new power variables, the power interaction of the Physical Element PE with the

external world can be described using the *power section* P shown in Figure 4(b): in the POG block schemes, the power sections are denoted by a dashed line, and the product of the two power variables v_e and v_f has the physical meaning of a power flowing through the section. Figure 5 shows, for each energetic domain, the Simscape graphical representation of the dynamic elements D_e , D_f and of the static elements R reported in Table 1. Each energetic domain is also characterized by two power variable generators: an *across generator* G_e producing as output an across power variable v_e and a *through generator* G_f producing as output a through power variable v_f . Figure 6 shows the Simscape graphical representation of the across and through generators D_e and D_f .

Modular Structure of the POG

The POG graphical representations of the dynamic elements D_e and D_f are shown in Figure 7(a) and Figure 7(b), respectively. These graphical representation respect the integral causality [4], since the the output power variables v_e (for D_e) and v_f (for D_f) exhibit an integral relationship with respect to the input power variables. The dynamic element D_e is characterized by the internal energy variable q_e , the input power variable v_f , the output power variable v_e , the constitutive relation $q_e = \Phi_e(v_e)$, and the differential equation $\dot{q}_e = v_f$. Conversely, the dynamic element D_f is characterised by the internal energy variable q_f , the input power variable v_e , the output power variable v_f , the constitutive relation $q_f = \Phi_f(v_f)$, and the differential equation $\dot{q}_f = v_e$. The integral causality is adopted in the

First Case Study: A DC Motor Driving an Hydraulic Pump

Figure S1 provides a schematic representation of the first case study, consisting in a DC motor driving an hydraulic pump [6].

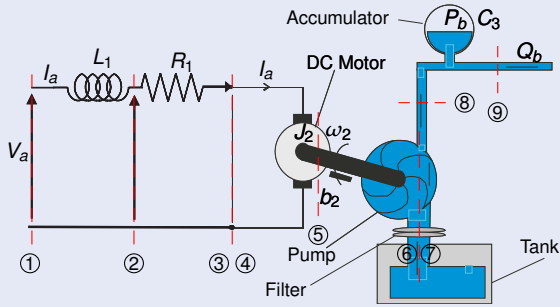


FIGURE S1 First Case Study: A DC motor driving an hydraulic pump. The electrical input power of the DC motor is given by $V_a I_a$. After some dissipation associated with the electrical resistance R_1 , the input power is converted into mechanical power, in order to drive the rotor inertia J_2 subject to the friction coefficient b_2 . The rotor of the DC motor is connected to an hydraulic pump, which pumps a volume flow rate Q_3 from a tank into an hydraulic capacitor C_3 (accumulator). The hydraulic output power flux is given by $P_b Q_b$.

The electrical part of the DC motor is composed of the stator inductor L_1 and stator resistance R_1 , respectively. The torque constant is then responsible for the power conversion from the electrical to the mechanical rotational domains, and viceversa. The electrical input power $V_a I_a$ is therefore converted to the mechanical domain, after some dissipation associated with the electrical resistance R_1 , while the mechanical dissipations are represented by the rotor friction coefficient b_2 . The hydraulic pump is responsible for converting the rotor movement, at angular speed ω_2 , into a volume flow rate Q_3 . Accounting for some dissipation which occurs in the hydraulic domain due to the hydraulic resistance R_3 , the volume flow rate is pumped from a tank into an hydraulic capacitor C_3 , which is denoted as Accumulator in Figure S1. The hydraulic output power is given by $P_b Q_b$, where P_b is the pressure within the hydraulic capacitor C_3 . The physical system in Figure S1 can be modeled using the POG block scheme of Figure S2. The first two elaboration blocks between power sections ① - ② and ② - ③ in the POG block scheme, describing the stator inductor L_1 and the resistor R_1 , are connected in series. Indeed, the respective summation nodes apply the following generalized VKL: $V_a'' = V_a - V_a'$ and $V_a' = V_1 + V_{R_1}$. The first connection block between power sections ③ - ④ describes the electrical/mechanical rotational power conversion associated with the torque constant K_{12} of the DC motor. The third and fourth elaboration blocks between power sections ④ - ⑤ and ⑤ - ⑥ in the POG block scheme of Figure S2, describing the

rotor inertia J_2 and the friction coefficient b_2 , are connected in parallel. Indeed, the respective summation nodes apply the following generalized CKL: $\tau_2'' = \tau_2 - \tau_2'$ and $\tau_2' = \tau_3 + \tau_{b_2}$. The second connection block between power sections ⑥ - ⑦ describes the mechanical rotational/hydraulic power conversion associated with the hydraulic pump coefficient K_{23} . The fifth and sixth elaboration blocks between power sections ⑦ - ⑧ and ⑧ - ⑨ in the POG block scheme, describing the hydraulic capacitor C_3 and the hydraulic resistor R_3 , are also connected in parallel. Indeed, the respective summation nodes apply the following generalized CKL: $Q_3'' = Q_3 - Q_3'$ and $Q_3' = Q_b + Q_{R_3}$.

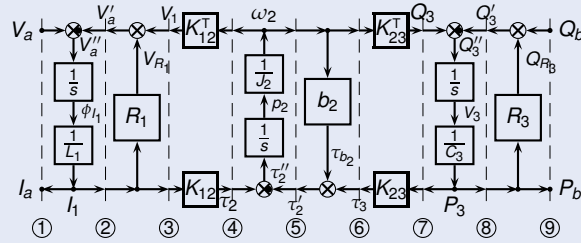


FIGURE S2 POG block scheme of the system in Figure S1. Starting from the left-hand side, the first two series-connected elaboration blocks describe the dynamics of the stator inductor L_1 and of the stator resistor R_1 . The first connection block characterized by the torque constant K_{12} describes the energy conversion between the electrical and mechanical rotational domains. The third and fourth parallel-connected elaboration blocks describe the dynamics of the rotor inertia J_2 and of its friction coefficient b_2 . The second connection block characterized by the hydraulic pump coefficient K_{23} describes the energy conversion between mechanical rotational and hydraulic domains. Finally, the fifth and sixth parallel-connected elaboration blocks describe the dynamics of the hydraulic capacitor C_3 and of the hydraulic resistor R_3 .

Figure S1 and Figure S2 also highlight the one-to-one correspondence between every single physical element L_1 , R_1 , K_{12} , J_2 , b_2 , K_{23} , C_3 , R_3 in the physical system and the blocks between the corresponding pair of power sections ①, ..., ⑨ in the POG block scheme. The POG block scheme of Figure S2 is in a one-to-one correspondence with the following state-space model:

$$\underbrace{\begin{bmatrix} L_1 & 0 & 0 \\ 0 & J_2 & 0 \\ 0 & 0 & C_3 \end{bmatrix}}_{\mathbf{L}} \underbrace{\begin{bmatrix} \dot{I}_1 \\ \dot{\omega}_2 \\ \dot{P}_3 \end{bmatrix}}_{\dot{\mathbf{x}}} = \underbrace{\begin{bmatrix} -R_1 & -K_{12} & 0 \\ K_{12} & -b_2 & -K_{23} \\ 0 & K_{23} & -R_3 \end{bmatrix}}_{\mathbf{A}} \underbrace{\begin{bmatrix} I_1 \\ \omega_2 \\ P_3 \end{bmatrix}}_{\mathbf{x}} + \underbrace{\begin{bmatrix} 1 & 0 \\ 0 & 0 \\ 0 & -1 \end{bmatrix}}_{\mathbf{B}} \underbrace{\begin{bmatrix} V_a \\ Q_b \end{bmatrix}}_{\mathbf{u}} \quad (\text{S1})$$

$$\underbrace{\begin{bmatrix} I_a \\ P_b \end{bmatrix}}_{\mathbf{y}} = \underbrace{\begin{bmatrix} 1 & 0 & 0 \\ 0 & 0 & 1 \end{bmatrix}}_{\mathbf{C}} \mathbf{x} + \underbrace{\begin{bmatrix} 0 & 0 \\ 0 & 0 \end{bmatrix}}_{\mathbf{D}} \underbrace{\begin{bmatrix} V_a \\ Q_b \end{bmatrix}}_{\mathbf{u}}$$

obtained by applying Property 4. System (S1) is in the POG state-space form S in (10).

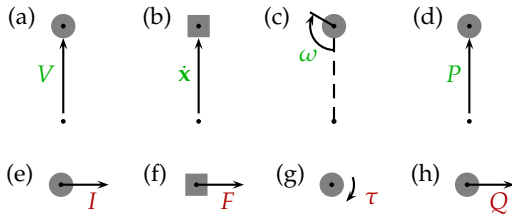


FIGURE 3 From (a) to (d): the voltage V , the velocity \dot{x} , the angular velocity ω , and the pressure P are defined between two points of the space. From (e) to (h): the current I , the force F , the torque τ and the volume flow rate Q are defined at each point of the space.

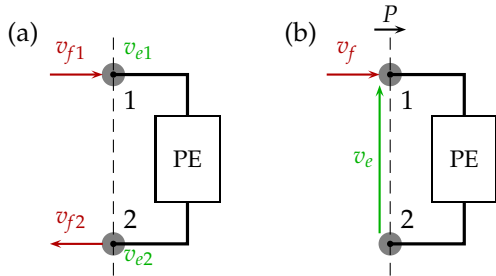


FIGURE 4 Physical element (PE) representations. (a) The two terminals of the PE are characterized by the pairs of power variables (v_{e1}, v_{f1}) and (v_{e2}, v_{f2}) . (b) An analogous representation of the physical element PE, where its interaction with other physical elements is described through the power section P characterized by the power variables (v_e, v_f) . The horizontal arrow located at the top of the power section indicates that the power P is positive when entering the system.

POG technique since the objective is to have block schemes that are suitable for simulation. The EBs in Figure 7(a) and Figure 7(b), describing the PEs D_e and D_f , respectively, are characterized by the following nonlinear integral relations:

$$\mathbf{v}_e = \Phi_e^{-1} \left(\int_0^t \mathbf{v}_f dt \right), \quad \mathbf{v}_f = \Phi_f^{-1} \left(\int_0^t \mathbf{v}_e dt \right),$$

which are graphically represented using the Laplace transform. The power variables and the constitutive relations in Figure 7 are boldface to denote the fact that they can be vectors and matrices, respectively, for the case of multidimensional dynamic elements D_e and D_f .

Two examples of this type is shown in the sidebars “Second Case Study: An Hydraulic Continuous Variable Transmission” and “Third Case Study: A Permanent Magnet Synchronous Motor”. The static element R can be graphically represented using the EB of Figure 7(c). In this case there is no integral causality issue, meaning that the static block R can be freely input-output inverted without any problem.

Whenever an energy conversion needs to be graphically represented, use can be made of the connection block of Figure 7(d). If the power variables x_1 and x_2 are of the same type, meaning that the power variables y_1 and y_2 are also of the same type, the connection block assumes the physical meaning of a *transformer*. Conversely, the connection

	Electrical	Mechanical Translational	Mechanical Rotational	Hydraulic
Physical Element D_e	Capacitor	Mass	Inertia	Hydraulic Capacitor
Physical Element D_f	Inductor	Spring	Rotational Spring	Hydraulic Inductor
Physical Element R	Resistor	Friction	Angular Friction	Hydraulic Resistor

FIGURE 5 Simscape graphical representation of the dynamic Physical Elements (PEs) D_e, D_f and of the static PEs R in the electrical, mechanical translational, mechanical rotational and hydraulic energetic domains. The PEs are shown using the representation proposed in Figure 4(b).

block is said to be a *gyrator*.

Series and Parallel Connections

A complex physical system can be composed of a large number of PEs, and can be modeled using a right combination of EBs and CBs. The PEs interact with each other and with the external world through series connections or parallel connections, as highlighted in Figure 13(a) and in Figure 13(b), respectively. As shown in Figure 4(a), each of the two PE terminals is characterized by a pair of power variables: (v_{e1}, v_{f1}) and (v_{e2}, v_{f2}) , respectively.

When the PE is connected in series, the effort power variables are related through the following relation $v_e = v_{e1} - v_{e2}$, which is named generalized Voltage Kirchoff’s Law (VKL). In this case, the three possible elaboration block configurations that can be obtained from Figure 7(b) are shown in Figure 14. Figure 14(a) shows the basic configuration for the series connection, characterized by the input power variables v_{e1} and v_{e2} and by the output power variables $v_{f1} = v_{f2}$. By inverting either the left or the

	Electrical	Mechanical Translational	Mechanical Rotational	Hydraulic
Across Generators G_e	 Voltage Generator	 Velocity Generator	 Angular Velocity Generator	 Pressure Generator
Through Generators G_f	 Current Generator	 Force Generator	 Torque Generator	 Flow Rate Generator

FIGURE 6 Simscape graphical representation of the across and through generators D_e and D_f in the electrical, mechanical translational, mechanical rotational and hydraulic energetic domains. The generators are shown using the representation proposed in Figure 4(b).

right power paths, the configurations of Figure 14(b) or Figure 14(c) are obtained, respectively. In the first case, the input power variables are v_{f1} and v_{e2} , while the output power variables are v_{e1} and v_{f2} . In the second case, the input power variables are v_{e1} and v_{f2} , while the output power variables are v_{f1} and v_{e2} . In order to respect the integral causality, from Figure 14 it is evident that: 1) the through dynamic elements D_f connected in series can only be graphically represented using the POG graphical representation shown in Figure 14(a); 2) the across dynamic elements D_e connected in series can be graphically represented using the two POG graphical representations shown in Figure 14(b) and Figure 14(c).

When the physical element is connected in parallel, the through power variables are related through the following relation $v_f = v_{f1} - v_{f2}$, which is named generalized Current Kirchhoff's Law (CKL). In this case, the three possible elaboration block configurations that can be obtained from Figure 7(a) are shown in Figure 15. Figure 15(a) shows the basic configuration, characterized by the input power variables v_{f1} and v_{f2} and by the output power variables $v_{e1} = v_{e2}$. By inverting either the left or the right power paths, the configurations of Figure 15(b) or Figure 15(c) are obtained, respectively. In the first case, the input power variables are v_{e1} and v_{f2} , while the output power variables are v_{e2} and v_{f1} . In the second case, the input power variables are v_{e2} and v_{f1} , while the output power variables are v_{e1} and v_{f2} . In order to respect the integral causality, from Figure 15 it is evident that: 1) the across dynamic

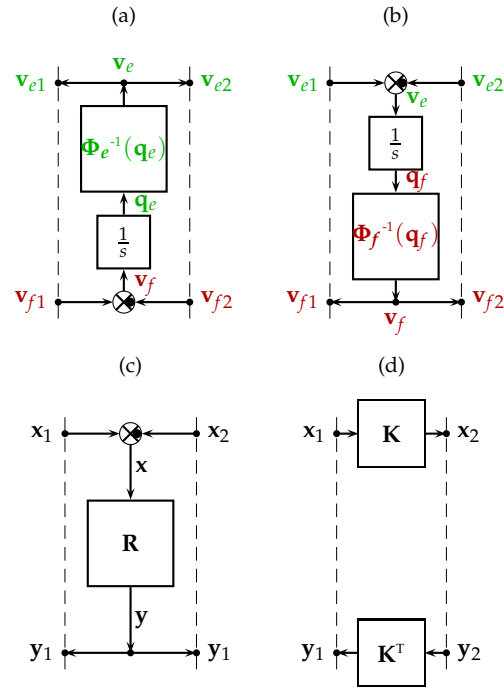


FIGURE 7 Elaboration Blocks (EBs) and Connection Blocks (CBs). (a) Basic EB describing the dynamic elements D_e . (b) Basic EB describing the dynamic elements D_f . (c) Basic EB describing the static elements R . (d) CB describing a power conversion occurring in the system. The power variables v_{e1} , v_{e2} , v_e , v_{f1} , v_{f2} , v_f in (a) and (b), as well as the inverted constitutive relations $\Phi_e^{-1}(q_e)$ and $\Phi_f^{-1}(q_f)$, are boldface to denote the fact that they can be vectors and matrices, respectively, for the case of multidimensional dynamic elements D_e and D_f . The same consideration applies to the power variables x_1 , x_2 , x , y_1 , y_2 , y , and to the matrices R , K in (c) and (d).

elements D_e connected in parallel can only be graphically represented using the POG graphical representation shown in Figure 15(a); 2) the through dynamic elements D_f connected in parallel can be graphically represented using the two POG graphical representations shown in Figure 15(b) and Figure 15(c).

Based on the previous considerations, the following three properties hold.

Property 1

Through dynamic elements D_f connected in series and across dynamic elements D_e connected in parallel only admit the EB configurations of Figure 14(a) and Figure 15(a), respectively. In the linear case, the EB configuration of Figure 14(a) translates into the configuration of Figure 16(A). The coefficient K characterizing the EB transfer function

$$v_f = \frac{1}{Ks} v_e$$

depends on the considered through dynamic element D_f connected in series: $K = L$ for the inductor, $K = E$ for the spring, $K = E_r$ for the rotational spring, $K = L_I$ for the

Second Case Study: An Hydraulic Continuous Variable Transmission

Figure S3 shows a schematic representation of the second case study, which is an hydraulic Continuous Variable Transmission (CVT) [35].

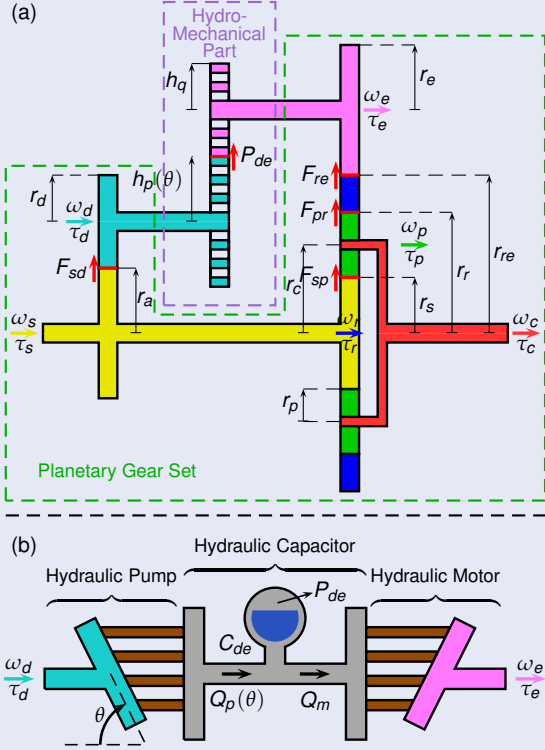


FIGURE S3 Second Case Study: An hydraulic Continuous Variable Transmission (CVT). (a) The structure of the hydraulic CVT system, which is composed of a planetary gear set and of a hydro-mechanical part. (b) The structure of the CVT hydro-mechanical part, which is composed of an hydraulic pump and an hydraulic motor charging and discharging an hydraulic capacitor C_{de} . The pressure P_{de} within the hydraulic capacitor C_{de} is function of the hydraulic pump volume flow rate $Q_p(\theta)$ and of the hydraulic motor volume flow rate Q_m : $C_{de}P_{de} = Q_p(\theta) - Q_m$.

The planetary gear set interacts with the other physical elements through the ring (blue element in Figure S3(a)), sun (yellow element), planetary (green elements), and carrier (red element) power sections, characterized by the power variables (ω_r, τ_r) , (ω_s, τ_s) , (ω_p, τ_p) , and (ω_c, τ_c) , respectively. The sun is connected to the hydraulic pump (light blue element), while the ring is connected to the hydraulic motor (pink element). The gears exchange the tangential forces F_{sp} , F_{pr} and F_{re} while elastically interacting with each other through the springs characterized by the stiffness coefficients K_{sp} , K_{pr} and K_{re} , and the sun exchanges the tangential force F_{sd} with the hydraulic pump while elastically interacting with it through the stiffness coefficients K_{sd} . As shown in Figure S3(b), the pressure P_{de} within the hydraulic capacitor C_{de} is a function of the hydraulic

pump volume flow rate $Q_p(\theta)$ and of the hydraulic motor volume flow rate Q_m as described by the following differential equation: $C_{de}\dot{P}_{de} = Q_p(\theta) - Q_m$. By controlling the tilt angle θ of the hydraulic pump plates, as highlighted in Figure S3(b), the hydraulic pressure P_{de} can be properly controlled.

The hydraulic CVT of Figure S3(a) can be modeled using the vectorial POG block scheme of Figure S4, which is said to be multidimensional since the matrices composing it contain more than one dynamic or static PE.

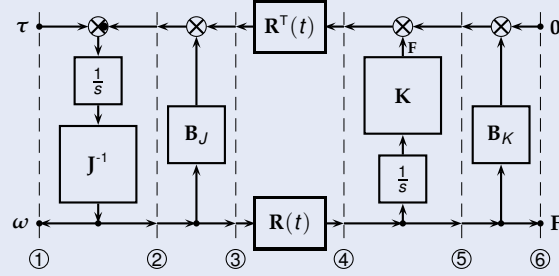


FIGURE S4 POG block scheme of the hydraulic CVT in Figure S3(a). Starting from the left-hand side, the first two parallel-connected elaboration blocks describe the dynamics of the rotational elements in matrix J , affected by the friction coefficients in matrix B_J . The connection block characterized by matrix $R(t)$ describes the energy conversions in the system, between the mechanical rotational/translational domains and between the mechanical rotational/hydraulic domains. The last two parallel-connected elaboration blocks describe the dynamics of the elastic and hydraulic elements in matrix K , affected by the dissipative terms in matrix B_K .

The parallel-connected elaboration blocks between power sections ① - ② and ② - ③, describing the mechanical rotational part of the system, are composed of the inertia and friction matrices J and B_J shown in (S2). The parallel-connected elaboration blocks between power sections ④ - ⑤ and ⑤ - ⑥, describing the mechanical translational and hydraulic parts of the system, are composed of the coupling and dissipative matrices K and B_K shown in (S2). The vectors τ , ω and F are also given in (S2), while the energy conversion matrix $R(t)$ between power sections ③ - ④ is given in (S3).

$$\omega = \begin{bmatrix} \omega_c \\ \omega_p \\ \omega_s \\ \omega_r \\ \omega_d \\ \omega_e \end{bmatrix}, \tau = \begin{bmatrix} \tau_c \\ \tau_p \\ \tau_s \\ \tau_r \\ \tau_d \\ \tau_e \end{bmatrix}, J = \begin{bmatrix} J_c & 0 & 0 & 0 & 0 & 0 \\ 0 & J_p & 0 & 0 & 0 & 0 \\ 0 & 0 & J_s & 0 & 0 & 0 \\ 0 & 0 & 0 & J_r & 0 & 0 \\ 0 & 0 & 0 & 0 & J_d & 0 \\ 0 & 0 & 0 & 0 & 0 & J_e \end{bmatrix}, B_J = \begin{bmatrix} b_c & 0 & 0 & 0 & 0 & 0 \\ 0 & b_p & 0 & 0 & 0 & 0 \\ 0 & 0 & b_s & 0 & 0 & 0 \\ 0 & 0 & 0 & b_r & 0 & 0 \\ 0 & 0 & 0 & 0 & b_d & 0 \\ 0 & 0 & 0 & 0 & 0 & b_e \end{bmatrix},$$

$$F = \begin{bmatrix} F_{sp} \\ F_{pr} \\ F_{sd} \\ F_{re} \\ P_{de} \end{bmatrix}, K = \begin{bmatrix} K_{sp} & 0 & 0 & 0 & 0 \\ 0 & K_{pr} & 0 & 0 & 0 \\ 0 & 0 & K_{sd} & 0 & 0 \\ 0 & 0 & 0 & K_{re} & 0 \\ 0 & 0 & 0 & 0 & C_{de}^{-1} \end{bmatrix}, B_K = \begin{bmatrix} d_{sp} & 0 & 0 & 0 & 0 \\ 0 & d_{pr} & 0 & 0 & 0 \\ 0 & 0 & d_{sd} & 0 & 0 \\ 0 & 0 & 0 & d_{re} & 0 \\ 0 & 0 & 0 & 0 & R_{de} \end{bmatrix}. \quad (S2)$$

$$\mathbf{R}(t) = \begin{bmatrix} -r_c & r_p & r_s & 0 & 0 & 0 \\ r_c & r_p & 0 & -r_r & 0 & 0 \\ 0 & 0 & r_a & 0 & r_d & 0 \\ 0 & 0 & 0 & r_{re} & 0 & r_e \\ 0 & 0 & 0 & 0 & h_p(\theta) & -h_q \end{bmatrix}. \quad (\text{S3})$$

The procedure to obtain the matrix $\mathbf{R}(t)$ from the schematics of the hydraulic CVT system shown in Figure S3 is described in [17]. The POG block scheme of Figure S4 is in a one-to-one correspondence with the following POG state-space model:

$$\underbrace{\begin{bmatrix} \mathbf{J} & \mathbf{0} \\ \mathbf{0} & \mathbf{K}^{-1} \end{bmatrix}}_{\mathbf{L}} \dot{\mathbf{x}} = \underbrace{\begin{bmatrix} -\mathbf{B}_J - \mathbf{R}^T(t) \mathbf{B}_K \mathbf{R}(t) & -\mathbf{R}^T(t) \\ \mathbf{R}(t) & \mathbf{0} \end{bmatrix}}_{\mathbf{A}(t)} \mathbf{x} + \underbrace{\begin{bmatrix} \mathbf{I} \\ \mathbf{0} \end{bmatrix}}_{\mathbf{B}} \underbrace{\mathbf{u}}_{\boldsymbol{\tau}} \quad (\text{S4})$$

$$\mathbf{y} = \mathbf{x} = \begin{bmatrix} \boldsymbol{\omega} \\ \mathbf{F} \end{bmatrix},$$

where the definition of the different matrices and vectors is given in (S2) and (S3). Model (S4) is obtained by applying Property 4, and is in the POG state-space form \mathbf{S} in (10). From the definition of the energy conversion matrix $\mathbf{R}(t)$ in (S3), it can be noticed that the coefficients handling the mechanical rotational/translational energy conversions are the radii of all the gears present in the hydraulic CVT system depicted in Figure S3(a), while the coefficients responsible for the mechanical rotational/hydraulic energy conversions are the coefficients $h_p(\theta)$ and h_q in Figure S3(a). Since the coefficient $h_p(\theta)$ is function of the time-variant tilt angle $\theta = \theta(t)$ of the hydraulic

pump plates, the energy conversion matrix $\mathbf{R}(t)$ is time-variant as well and, consequently, the considered hydraulic CVT system exhibits a time-variant nature.

By disregarding the gears elastic interaction and the hydraulic capacitor, namely by letting $\mathbf{K} \rightarrow \infty$ and $C_{de} \rightarrow 0$, from the first equation in (S4) the set $\mathbf{R}(t)\boldsymbol{\omega} = \mathbf{0}$ of vectorial constraints can be obtained. The latter constraint implies that the speed vector $\boldsymbol{\omega}$ can be expressed as a function of a new reduced speed vector $\hat{\mathbf{x}}$ of the reduced-order system: $\boldsymbol{\omega} = \mathbf{Q}_1(t)\hat{\mathbf{x}}$. Choosing $\hat{\mathbf{x}} = \boldsymbol{\omega}_s$, the following can be written:

$$\underbrace{\begin{bmatrix} \boldsymbol{\omega} \\ \mathbf{F} \end{bmatrix}}_{\mathbf{x}} = \underbrace{\begin{bmatrix} \mathbf{Q}(t) \\ \mathbf{0} \end{bmatrix}}_{\mathbf{T}(t)} \underbrace{\hat{\mathbf{x}}}_{\boldsymbol{\omega}_s}, \quad \text{where } \mathbf{Q}(t) = \begin{bmatrix} \frac{h_q r_d r_{re} r_s + K_p r_a r_r r \theta}{2 h_q r_d r_{re} r_c} \\ \frac{K_p r_a r_r r \theta - h_q r_d r_{re} r_s}{2 h_q r_d r_p r_{re}} \\ 1 \\ \frac{K_p r_a r_{re} \theta}{h_q r_d r_{re}} \\ -\frac{r_a}{r_d} \\ -\frac{K_p r_a \theta}{h_q r_d} \end{bmatrix}. \quad (\text{S5})$$

The congruent transformation $\mathbf{x} = \mathbf{T}(t)\hat{\mathbf{x}}$ in (S5) is a particular case, when $\mathbf{T}_u = \mathbf{0}$, of the congruent transformation defined in (18). This congruent time-variant transformation relates the state vector \mathbf{x} of the original hydraulic CVT model (S4) to the chosen new state vector $\hat{\mathbf{x}} = \boldsymbol{\omega}_s$ of the reduced-order hydraulic CVT model. By applying the transformation $\mathbf{x} = \mathbf{T}(t)\hat{\mathbf{x}}$ in (S5) to system (S4), the following reduced state-space time-variant model of the hydraulic CVT can be obtained:

$$\hat{\mathbf{L}}(t) \dot{\hat{\mathbf{x}}} = \hat{\mathbf{A}}(t) \hat{\mathbf{x}} + \hat{\mathbf{B}}(t) \boldsymbol{\tau}, \quad (\text{S6})$$

where the new system matrices $\hat{\mathbf{L}}(t)$, $\hat{\mathbf{A}}(t)$, and $\hat{\mathbf{B}}(t)$ are computed as described in (19).

hydraulic inductor. Similarly, the EB configuration of Figure 15(a) translates into the configuration of Figure 16(B). The coefficient K characterizing the EB transfer function

$$v_e = \frac{1}{K_s} v_f$$

depends on the considered through dynamic element D_e connected in parallel: $K = C$ for the capacitor, $K = M$ for the mass, $K = J$ for the inertia, $K = C_I$ for the hydraulic capacitor.

Property 2

Through dynamic elements D_f connected in parallel and across dynamic elements D_e connected in series admit two EB configurations: those of Figure 15(b)-(c) and Figure 14(b)-(c), respectively. In the linear case, the EB configurations of Figure 15(b)-(c) translate into the configurations of Figure 17(A)-(B). Similarly, the EB configurations of Figure 14(b)-(c) translate into the configurations of Figure 17(C)-(D).

Property 3

Static elements R admit all the possible EB configurations shown in Figure 14 and in Figure 15 for the series and parallel connections, respectively. This follows from the fact that static elements are not characterized by differential equations, and therefore do not exhibit the integral causality issue.

From Figure 14, Figure 15, Figure 16, and Figure 17, it can be concluded that the symbolism of the POG technique is composed of standard blocks that can be found in standard Simulink libraries, which makes this technique particularly suitable and intuitive for non-expert users.

POG State-Space Model

A system \mathbf{S} in a POG state-space representation has the following structure:

$$\mathbf{S} = \begin{cases} \mathbf{L} \dot{\mathbf{x}} = \mathbf{A} \mathbf{x} + \mathbf{B} \mathbf{u}, \\ \mathbf{y} = \mathbf{C} \mathbf{x} + \mathbf{D} \mathbf{u}, \end{cases} \quad (\text{10})$$

Third Case Study: A Permanent Magnet Synchronous Motor

Figure S5 shows a schematic representation of the third case study, which is a Permanent Magnet Synchronous Motor (PMSM) [21].

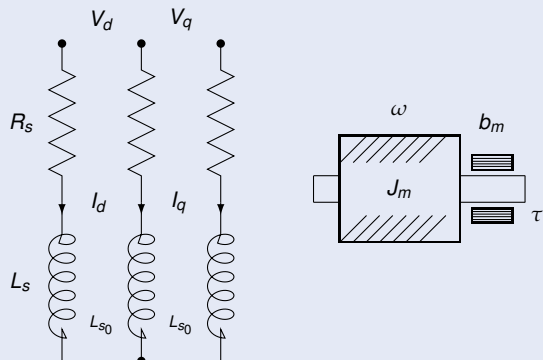


FIGURE S5 Third Case Study: A Permanent Magnet Synchronous Motor (PMSM). On the left: the electrical part of the PMSM, composed of the stator phase inductors L_s , which are mutually coupled through the mutual inductors coefficient having maximum value L_{s0} , and of the stator phases resistors R_s . On the right: the mechanical part of the PMSM, composed of the rotor inertia J_m rotating at angular speed ω , subject to the friction coefficient b_m and to the load torque τ .

The electrical part of the PMSM is composed of the stator phase inductors and resistors: L_s and R_s , respectively. The inductors L_s are mutually coupled through the mutual inductance coefficient having maximum value L_{s0} . The input electrical power in the d-q reference frame is given by $\mathbf{V}^T \mathbf{I}$, where the voltage and current vectors \mathbf{V} and \mathbf{I} are given by:

$$\mathbf{V} = \begin{bmatrix} V_d \\ V_q \end{bmatrix}, \quad \text{and} \quad \mathbf{I} = \begin{bmatrix} I_d \\ I_q \end{bmatrix}, \quad (\text{S7})$$

and is then converted to the mechanical rotational domain, after the impact of the stator dynamics and some dissipation associated with the electrical resistors R_s . The resulting output power flux is given by $\omega \tau$, being ω and τ the rotor angular speed and load torque, respectively, after the impact of the rotor dynamics and some dissipation associated with the rotor friction coefficient b_m .

The physical system in Figure S5 can be modeled using the POG block scheme shown in Figure S6. As observed in the sidebar “Second Case Study: An Hydraulic Continuous Variable Transmission”, even in this case it is remarkable to notice that, if the input and output variables of a POG block scheme are multidimensional, as for the voltage and current vectors \mathbf{V} and \mathbf{I} in (S7), the involved elaboration and connection blocks become multidimensional as well. In fact, the series-connected elaboration blocks between power sections ① - ② and ② - ③, describing the electrical part of the system, are

composed of the matrices \mathbf{L}_e and \mathbf{L}_{en} defined in (S8). The elaboration block between power sections ③ - ④, describing the dissipation taking place in the electrical part of the PMSM, is composed of the resistance matrix \mathbf{R}_e defined in (S8).

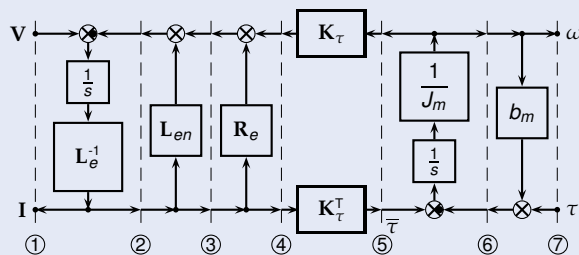


FIGURE S6 POG block scheme of the Permanent Magnet Synchronous Motor schematized in Figure S5. Starting from the left-hand side, the first three series-connected elaboration blocks describe the dynamics of the electric part, which is characterized by the dynamic elements in matrices \mathbf{L}_e and \mathbf{L}_{en} and by the static elements in matrix \mathbf{R}_e . The connection block characterized by vector $\mathbf{K}_\tau = [K_d \ K_q]^T$ describes the energy conversion between the electrical and the mechanical rotational energetic domains. The last two parallel-connected elaboration blocks describe the dynamics of the mechanical part, characterized by the rotor inertia J_m and by the friction coefficient b_m .

The matrices \mathbf{L}_e , \mathbf{L}_{en} and \mathbf{R}_e are defined as:

$$\mathbf{L}_e = \begin{bmatrix} \rho L_e & 0 \\ 0 & \rho L_e \end{bmatrix}, \quad \mathbf{L}_{en} = \begin{bmatrix} 0 & -\rho^2 \omega L_e \\ \rho^2 \omega L_e & 0 \end{bmatrix}, \quad \mathbf{R}_e = \begin{bmatrix} -\rho R_s & 0 \\ 0 & -\rho R_s \end{bmatrix}, \quad (\text{S8})$$

where $L_e = L_s + \frac{L_{s0}}{2}$, L_s is the auto-inductance coefficient, and ρ is the number of polar pairs. The connection block between power sections ④ - ⑤, describing the energy conversion between the electrical and mechanical rotational domains, is composed of the torque vector $\mathbf{K}_\tau = [K_d \ K_q]^T$. It is in correspondence of this connection block that the energy conversion between the two-dimensional electrical part and the one-dimensional mechanical part of the PMSM occurs: the parallel-connected elaboration blocks between power sections ⑤ - ⑥ and ⑥ - ⑦ are no longer two-dimensional, but one-dimensional instead. These two elaboration blocks describe the mechanical rotational part of the system, and are composed of the rotor inertia J_m and of the rotor friction coefficient b_m .

The POG block scheme of Figure S6 is in a one-to-one correspondence with the following state-space model:

$$\underbrace{\begin{bmatrix} \mathbf{L}_e & 0 \\ 0 & J_m \end{bmatrix}}_{\mathbf{L}} \underbrace{\begin{bmatrix} \dot{\mathbf{I}} \\ \dot{\omega} \end{bmatrix}}_{\mathbf{x}} = \underbrace{\begin{bmatrix} \mathbf{L}_{en} + \mathbf{R}_e & -\mathbf{K}_\tau \\ \mathbf{K}_\tau^T & -b_m \end{bmatrix}}_{\mathbf{A}} \underbrace{\begin{bmatrix} \mathbf{I} \\ \omega \end{bmatrix}}_{\mathbf{x}} + \underbrace{\begin{bmatrix} 1 & 0 \\ 0 & -1 \end{bmatrix}}_{\mathbf{B}} \underbrace{\begin{bmatrix} \mathbf{V} \\ \tau \end{bmatrix}}_{\mathbf{u}}, \quad (\text{S9})$$

and $\mathbf{y} = \mathbf{x}$ and $\mathbf{D} = 0$. System (S9) is obtained by applying Property 4, and is in the POG state-space form \mathbf{S} defined in (10).

The dynamics of the PMSM can also be expressed in the static reference frame starting from the model of Figure S6 by using a proper transformation [21], thus allowing effective simulations of the PMSM in the static frame as well. A simulation example is shown in Figure S7, where the PMSM is simulated using the parameters available from the dataset in [21]. In this case, a speed control using a proportional-integral-derivative regulator is applied to the PMSM, in order to make the rotor speed ω track the desired speed profile ω_d shown in Figure S7(a):

$$\bar{\tau}_d = K_p \left(1 + T_d s + \frac{1}{T_i s} \right) (\omega_d - \omega),$$

where K_p , T_d and T_i are the proportional action and the time constants of the derivative and integral actions, respectively, and are set as the dataset in [21]. In the simulation of Figure S7, the PMSM is supposed to be subject to a load torque $\tau = 200$ Nm. Figure S7(b) shows that the actual motive torque $\bar{\tau}$ properly tracks the desired profile $\bar{\tau}_d$, resulting in the rotor speed ω properly tracking the desired profile ω_d , as shown in Figure S7(a). Figure S7(c) and Figure S7(d) report the three-phase voltages and currents in the static frame in a zoomed-in time interval, showing the detailed simulations that can be performed starting from the PMSM model of Figure S6.

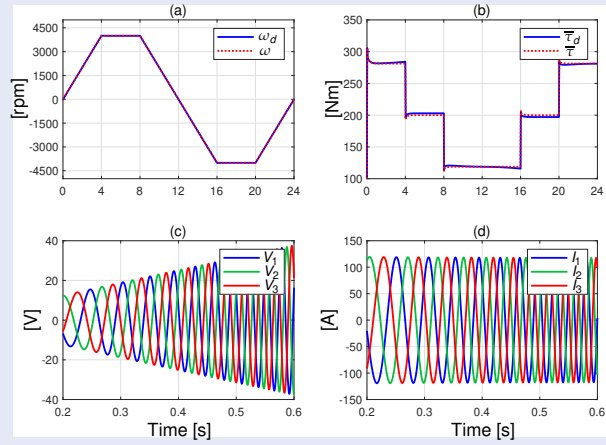


FIGURE S7 Simulation of the Permanent Magnet Synchronous Motor (PMSM). A speed control is applied to the PMSM in order to make the rotor speed track the desired profile while subject to a load torque. (a) The desired and actual rotor speeds ω_d and ω . (b) The desired and actual motive torques $\bar{\tau}_d$ and $\bar{\tau}$. (c) The three-phase voltages V_1 , V_2 , and V_3 . (d) The three-phase currents I_1 , I_2 , and I_3 .

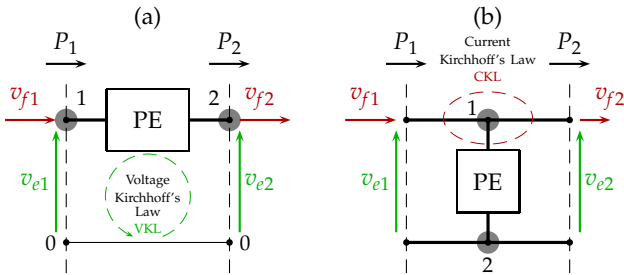


FIGURE 13 Connections of the Physical Elements (PEs) with each other or with the external world. (a) For what concerns a PE connected in series, $v_e = v_{e1} - v_{e2}$ holds, where such relation is named generalized Voltage Kirchhoff's Law (VKL). (b) For what concerns a PE connected in parallel, $v_f = v_{f1} - v_{f2}$ holds, where such relation is named generalized Current Kirchhoff's Law (CKL).

where \mathbf{L} is the energy matrix, \mathbf{A} is the power matrix, \mathbf{B} is the input power matrix, \mathbf{C} is the output matrix, and \mathbf{D} is the input/output matrix. For a system \mathbf{S} in a POG state-space form as in (10), matrix $\mathbf{L} = \mathbf{L}^T \geq 0$ is always a symmetric semidefinite matrix. Furthermore, the names *energy* and *power* matrices, for matrices \mathbf{L} and \mathbf{A} , come from the fact that they allow to compute the energy E_s stored within the system and the power P_d dissipated within the system, respectively, as follows:

$$E_s = \frac{1}{2} \mathbf{x}^T \mathbf{L} \mathbf{x} \geq 0, \quad \text{and} \quad P_d = \mathbf{x}^T \mathbf{A} \mathbf{x} = \mathbf{x}^T \mathbf{A}_s \mathbf{x}, \quad (11)$$

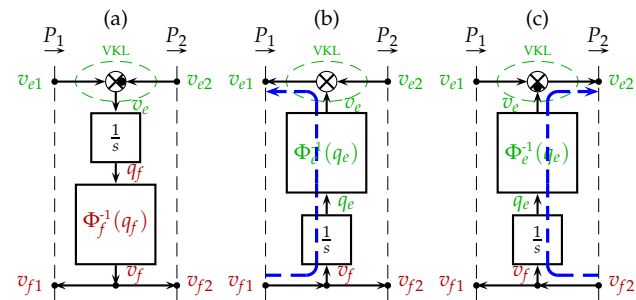


FIGURE 14 Elaboration Block configurations of physical elements connected in series. (a) Basic configuration, where v_{e1} and v_{e2} are the input power variables while v_{f1} and v_{f2} are the output power variables. (b) This configuration can be obtained from (a) by inverting the path highlighted by the blue arrow. In this case, v_{f1} and v_{e2} are the input power variables while v_{e1} and v_{f2} are the output power variables. (c) This configuration can be obtained from (a) by inverting the path highlighted by the blue arrow. In this case, v_{e1} and v_{f2} are the input power variables while v_{f1} and v_{e2} are the output power variables.

where $\mathbf{A}_s = \frac{\mathbf{A} + \mathbf{A}^T}{2}$ is the symmetric part of matrix \mathbf{A} . In the POG state-space representation (10), the matrix \mathbf{L} is always a symmetric and positive semidefinite matrix, as opposed to the so-called descriptor state-space model [57]. A system \mathbf{S} in the POG state-space form (10) can always be converted into a system $\bar{\mathbf{S}}$ in a classical state-space form

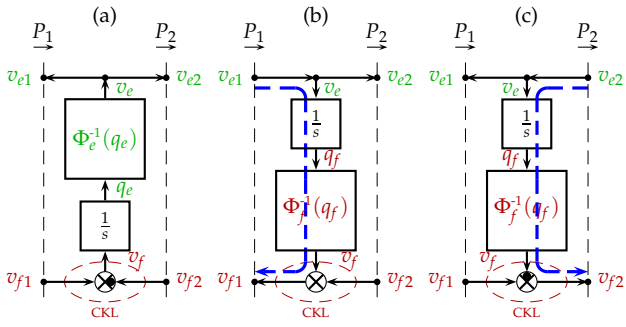


FIGURE 15 Elaboration Block configurations of physical elements connected in parallel. (a) Basic configuration, where v_{f1} and v_{f2} are the input power variables while v_{e1} and v_{e2} are the output power variables. (b) This configuration can be obtained from (a) by inverting the path highlighted by the blue arrow. In this case, v_{e1} and v_{f2} are the input power variables while v_{f1} and v_{e2} are the output power variables. (c) This configuration can be obtained from (a) by inverting the path highlighted by the blue arrow. In this case, v_{f1} and v_{e2} are the input power variables while v_{e1} and v_{f2} are the output power variables.

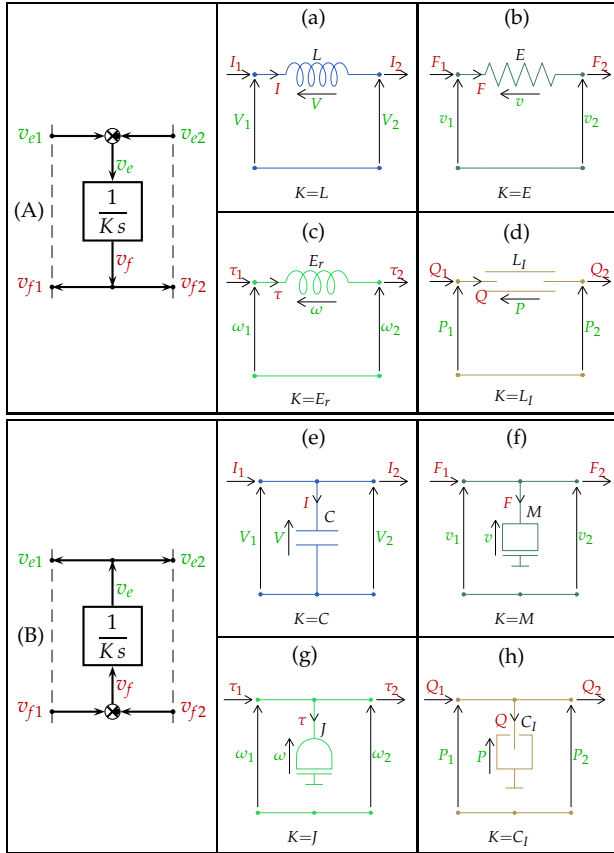


FIGURE 16 Dynamic Physical Elements (PEs) admitting one Elaboration Block (EB) configuration only. (A) EB configuration for the through dynamic elements D_f connected in series: inductor L (a), spring E (b), rotational spring E_r (c), and hydraulic inductor L_l (d). (B) EB configuration for the across dynamic elements D_e connected in parallel: capacitor C (e), mass M (f), inertia J (g), and hydraulic capacitor C_l (h).

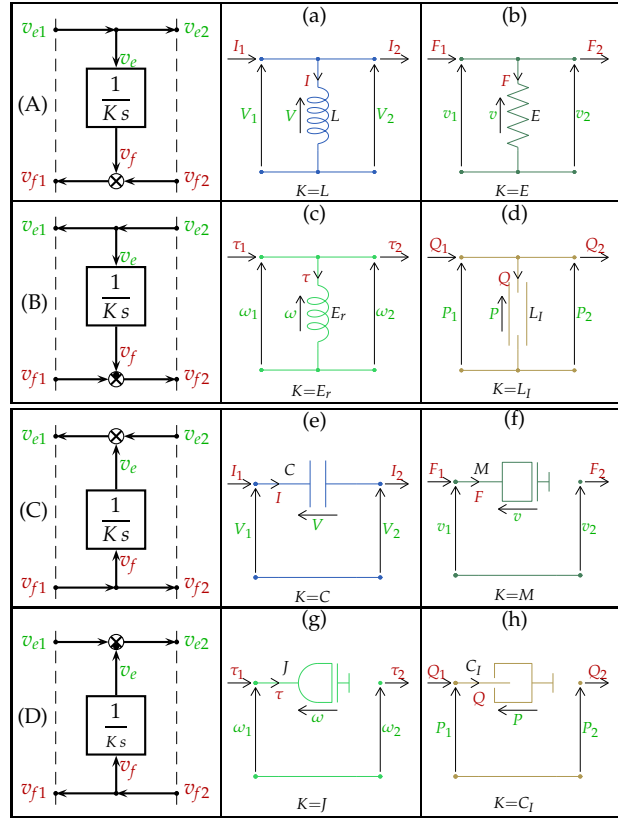


FIGURE 17 Dynamic Physical Elements (PEs) admitting two Elaboration Block (EB) configurations. (A) and (B) EB configurations for the through dynamic elements D_f connected in parallel: inductor L (a), spring E (b), rotational spring E_r (c), and hydraulic inductor L_l (d). (C) and (D) EB configuration for the across dynamic elements D_e connected in series: capacitor C (e), mass M (f), inertia J (g), and hydraulic capacitor C_l (h).

by performing the following transformations:

$$\mathbf{S} = \begin{cases} \dot{\mathbf{x}} = \underbrace{\mathbf{L}^{-1}\mathbf{A}}_{\bar{\mathbf{A}}} \mathbf{x} + \underbrace{\mathbf{L}^{-1}\mathbf{B}}_{\bar{\mathbf{B}}} \mathbf{u}, \\ \mathbf{y} = \mathbf{C}\mathbf{x} + \mathbf{D}\mathbf{u}, \end{cases} \Leftrightarrow \bar{\mathbf{S}} = \begin{cases} \dot{\mathbf{x}} = \bar{\mathbf{A}}\mathbf{x} + \bar{\mathbf{B}}\mathbf{u}, \\ \mathbf{y} = \mathbf{C}\mathbf{x} + \mathbf{D}\mathbf{u}. \end{cases} \quad (12)$$

Additionally, it can be proven that the input/output transfer matrix $\mathbf{H}(s)$ can always be obtained from \mathbf{S} in (10) and from $\bar{\mathbf{S}}$ in (12) as follows:

$$\mathbf{H}(s) = \mathbf{C}(\mathbf{L}s - \mathbf{A})^{-1}\mathbf{B} + \mathbf{D} = \mathbf{C}(\mathbf{I}s - \bar{\mathbf{A}})^{-1}\bar{\mathbf{B}} + \mathbf{D}.$$

Furthermore, the following property holds.

Property 4

From a linear POG block scheme, the matrices \mathbf{L} , \mathbf{A} , \mathbf{B} , \mathbf{C} and \mathbf{D} of the POG state-space model \mathbf{S} in (10) can always be read by direct inspection of the POG block scheme itself, as described in the following.

Property 4 is described by referring to the system in Figure S1 of the sidebar “First case study: A DC Motor

The symbolism of the POG technique is composed of standard blocks available in standard Simulink libraries, which makes this technique particularly suitable and intuitive for non-expert users.

Driving an Hydraulic Pump". Let n be the number of dynamic elements D_e and D_f in the system, and let m be the number of inputs and outputs, defining the dimensions of the state, input and output vectors $\mathbf{x} \in \mathbb{R}^{n \times 1}$, $\mathbf{u}, \mathbf{y} \in \mathbb{R}^{m \times 1}$ of system \mathbf{S} in (10), respectively. The components x_i of the state vector \mathbf{x} must be chosen equal to the output power variables of the dynamic elements that are present in the system. For the system under consideration, $n = 3$ and $m = 2$ hold, and the state, input, and output vectors are $\mathbf{x} = [I_1 \ \omega_2 \ P_3]^T$, $\mathbf{u} = [V_a \ Q_b]^T$, and $\mathbf{y} = [I_a \ P_b]^T$. The coefficients of the system matrices $\mathbf{L}, \mathbf{A}, \mathbf{B}, \mathbf{C}$ and \mathbf{D} in (10) can be directly read by direct inspection of the POG block scheme as follows. 1) the l_{ii} element of the diagonal matrix $\mathbf{L} \in \mathbb{R}^{n \times n}$, for $i \in 1, \dots, n$, is given by the coefficient characterizing the i -th PE. For the system in Figure S1, the elements l_{ii} of the diagonal matrix \mathbf{L} are L_1, J_2 and C_3 , as shown by the resulting matrix \mathbf{L} in (S1). 2) The a_{ij} element of matrix $\mathbf{A} \in \mathbb{R}^{n \times n}$ is the *global gain* of the static paths linking the j -th state variables x_j to the input of the integrator associated with the i -th PE, for $i, j \in 1, \dots, n$. Note that the *global gain* is the sum of the gains of all the static paths connecting the two considered points. For example, the static path linking the first state variable I_1 in Figure S2 to the integrator of L_1 is $-R_1$, forming the a_{11} element of the resulting matrix \mathbf{A} in (S1). 3) The b_{ij} element of matrix $\mathbf{B} \in \mathbb{R}^{n \times m}$ is the global gain of the static paths linking the j -th input variable u_j to the integrator of the i -th PE, for $i \in 1, \dots, n$ and $j \in 1, \dots, m$. For example, the path linking the first input variable V_a in Figure S2 to the integrator of L_1 is 1, forming the b_{11} element of the resulting matrix \mathbf{B} in (S1). 4) The c_{ij} element of matrix $\mathbf{C} \in \mathbb{R}^{m \times n}$ is the global gain of the static paths linking the j -th state variable x_j to the i -th output variable y_i , for $i \in 1, \dots, m$ and $j \in 1, \dots, n$. For example, the path linking the first state variable I_1 in Figure S2 to first output variable I_a is 1, as $I_1 = I_a$. This forms the c_{11} element of the resulting matrix \mathbf{C} in (S1). 5) The d_{ij} element of matrix $\mathbf{D} \in \mathbb{R}^{m \times m}$ is the global gain of the static paths linking the j -th input variable to the i -th output variable, for $i, j \in 1, \dots, m$. For example, the path linking the first input variable V_a in Figure S2 to first output variable I_a is 0, as no such path exists. This forms the d_{11} element of the resulting matrix \mathbf{D} in (S1).

Other three examples of application of Property 4 can be

found in the sidebars "Second Case Study: An Hydraulic Continuously Variable Transmission", "Third Case Study: A Permanent Magnet Synchronous Motor", and "Fourth Case Study: An Hydraulic Clutch".

Congruent State-Space Transformations and Model Reduction

The typical type of state-space transformation that can be applied to a system $\bar{\mathbf{S}}$ in the classical state-space form (12) is a *similitude* transformation $\mathbf{x} = \mathbf{T}\tilde{\mathbf{x}}$, which transforms system $\bar{\mathbf{S}}$ into the transformed system $\hat{\mathbf{S}}$ as follows:

$$\bar{\mathbf{S}} = \begin{cases} \dot{\mathbf{x}} = \bar{\mathbf{A}}\mathbf{x} + \bar{\mathbf{B}}\mathbf{u} \\ \mathbf{y} = \mathbf{C}\mathbf{x} + \mathbf{D}\mathbf{u} \end{cases} \xrightarrow{\mathbf{x}=\mathbf{T}\tilde{\mathbf{x}}} \hat{\mathbf{S}} = \begin{cases} \dot{\tilde{\mathbf{x}}} = \tilde{\mathbf{A}}\tilde{\mathbf{x}} + \tilde{\mathbf{B}}\mathbf{u} \\ \mathbf{y} = \tilde{\mathbf{C}}\tilde{\mathbf{x}} + \mathbf{D}\mathbf{u} \end{cases}, \quad (16)$$

where the matrices of the transformed system $\hat{\mathbf{S}}$ are:

$$\tilde{\mathbf{A}} = \mathbf{T}^{-1}[\bar{\mathbf{A}}\mathbf{T} - \dot{\mathbf{T}}], \quad \tilde{\mathbf{B}} = \mathbf{T}^{-1}\bar{\mathbf{B}}, \quad \tilde{\mathbf{C}} = \mathbf{C}\mathbf{T}. \quad (17)$$

In this case, the transformation matrix \mathbf{T} must be square, not singular and can be, in general, time-variant, even though its explicit dependence "(t)" on time is not shown in (16) for simplicity of notation. On the other hand, a system \mathbf{S} in the POG state-space form as in (10) can be transformed into a new POG system $\hat{\mathbf{S}}$ using the *congruent* transformation $\mathbf{x} = \mathbf{T}\mathbf{z} + \mathbf{T}_u\mathbf{u}$ as follows:

$$\mathbf{S} = \begin{cases} \mathbf{L}\dot{\mathbf{x}} = \mathbf{A}\mathbf{x} + \mathbf{B}\mathbf{u} \\ \mathbf{y} = \mathbf{C}\mathbf{x} + \mathbf{D}\mathbf{u} \end{cases} \xrightarrow{\mathbf{x}=\mathbf{T}\hat{\mathbf{x}}+\mathbf{T}_u\mathbf{u}} \hat{\mathbf{S}} = \begin{cases} \hat{\mathbf{L}}\dot{\hat{\mathbf{x}}} = \hat{\mathbf{A}}\hat{\mathbf{x}} + \hat{\mathbf{B}}\mathbf{u} \\ \mathbf{y} = \hat{\mathbf{C}}\hat{\mathbf{x}} + \hat{\mathbf{D}}\mathbf{u} \end{cases} \quad (18)$$

where the new matrices of system $\hat{\mathbf{S}}$ are defined as follows:

$$\hat{\mathbf{L}} = \mathbf{T}^T\mathbf{L}\mathbf{T}, \quad \hat{\mathbf{A}} = \mathbf{T}^T[\mathbf{A}\mathbf{T} - \mathbf{L}\dot{\mathbf{T}}], \quad (19)$$

$$\hat{\mathbf{B}} = \mathbf{T}^T[\mathbf{A}\mathbf{T}_u + \mathbf{B}], \quad \hat{\mathbf{C}} = \mathbf{C}\mathbf{T}, \quad \hat{\mathbf{D}} = \mathbf{C}\mathbf{T}_u + \mathbf{D},$$

supposing \mathbf{T}_u constant and $\mathbf{T}^T\mathbf{L}\dot{\mathbf{T}}_u = 0$. Note that, in the case of congruent transformations, matrix \mathbf{T} can also be rectangular and not full rank. The utility of congruent state-space transformations within the POG technique becomes evident when considering model reduction. When an eigenvalue of the energy matrix \mathbf{L} tends to zero or to infinite, the system model degenerates to a lower dimension, and the matrices of the reduced-order model can be obtained using (19) by properly defining the matrices \mathbf{T} and \mathbf{T}_u of the state-space congruent transformation $\mathbf{x} = \mathbf{T}\hat{\mathbf{x}} + \mathbf{T}_u\mathbf{u}$. Two examples of model reduction using this technique can be found in the sidebars "Second Case Study: An Hydraulic Continuously Variable Transmission" and "Fourth Case Study: An Hydraulic Clutch".

Fourth Case Study: An Hydraulic Clutch

Figure S8 shows a schematic representation of the fourth case study, which is an hydraulic clutch.

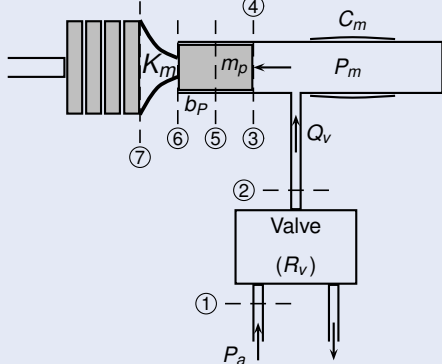


FIGURE S8 Fourth Case Study: An hydraulic clutch. The supply pressure P_a generates the volume flow rate Q_v entering the hydraulic capacitor C_m through an hydraulic resistor (valve) R_v . The pressure P_m originating within the hydraulic capacitor C_m pushes the piston having mass m_p subject to friction b_p . The piston movement in turn compresses the mechanical spring characterized by stiffness K_m , generating the compression of the clutch plates locking the clutch.

By controlling the supply pressure P_a , or by modulating the hydraulic resistor R_v , the volume of fluid within

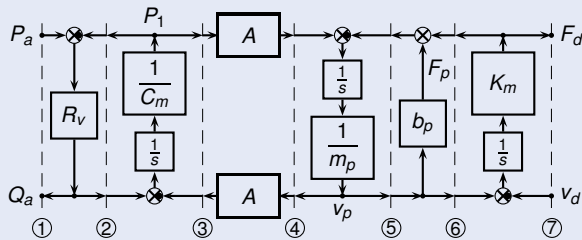


FIGURE S9 POG block scheme of the Hydraulic clutch in Figure S8. Starting from the left-hand side, the first two elaboration blocks describe the hydraulic resistance (valve) R_v and the hydraulic capacitor C_m . The following connection block handles the energy conversion from the hydraulic to the mechanical translational mechanical domain and viceversa. The next three elaboration blocks describe the piston mass m_p , the piston friction coefficient b_p and the spring stiffness K_m .

the hydraulic capacitor C_m can be properly controlled, thus controlling the movement of the piston m_p and, consequently, the compression of the clutch plates by means of the mechanical spring K_m .

The physical system in Figure S8 can be modeled using the POG block scheme shown in Figure S9, which is in a one-to-one correspondence with the following POG state-space model:

$$\underbrace{\begin{bmatrix} C_m & 0 & 0 \\ 0 & m_p & 0 \\ 0 & 0 & \frac{1}{K_m} \end{bmatrix}}_{\mathbf{L}} \dot{\mathbf{x}} = \underbrace{\begin{bmatrix} -R_v & -A & 0 \\ A & -b_p & -1 \\ 0 & 1 & 0 \end{bmatrix}}_{\mathbf{A}} \underbrace{\begin{bmatrix} P_m \\ v_p \\ F_m \end{bmatrix}}_{\mathbf{x}} + \underbrace{\begin{bmatrix} R_v & 0 \\ 0 & 0 \\ 0 & -1 \end{bmatrix}}_{\mathbf{B}} \underbrace{\begin{bmatrix} P_a \\ v_d \end{bmatrix}}_{\mathbf{u}},$$

$$\underbrace{\begin{bmatrix} Q_a \\ F_d \end{bmatrix}}_{\mathbf{y}} = \underbrace{\begin{bmatrix} -R_v & 0 & 0 \\ 0 & 0 & 1 \end{bmatrix}}_{\mathbf{C}} \mathbf{x} + \underbrace{\begin{bmatrix} R_v & 0 \\ 0 & 0 \end{bmatrix}}_{\mathbf{D}} \mathbf{u}. \quad (\text{S10})$$

The hydraulic capacitance C_m is usually very small, meaning that it can be neglected in order to reduce the system dimension. For this purpose, the following state-space congruent transformation

$$\underbrace{\begin{bmatrix} P_m \\ v_p \\ F_m \end{bmatrix}}_{\mathbf{x}} = \underbrace{\begin{bmatrix} -\frac{A}{R_v} & 0 \\ 1 & 0 \\ 0 & 1 \end{bmatrix}}_{\mathbf{T}} \underbrace{\begin{bmatrix} v_p \\ F_m \end{bmatrix}}_{\hat{\mathbf{x}}} + \underbrace{\begin{bmatrix} 1 & 0 \\ 0 & 0 \\ 0 & 0 \end{bmatrix}}_{\mathbf{T}_u} \underbrace{\begin{bmatrix} P_a \\ v_d \end{bmatrix}}_{\mathbf{u}} \quad (\text{S11})$$

can be applied to system (S10), leading to the following reduced-order system:

$$\underbrace{\begin{bmatrix} m_p & 0 \\ 0 & \frac{1}{K_m} \end{bmatrix}}_{\hat{\mathbf{L}}} \dot{\hat{\mathbf{x}}} = \underbrace{\begin{bmatrix} -b_p - \frac{A^2}{R_v} & -1 \\ 1 & 0 \end{bmatrix}}_{\hat{\mathbf{A}}} \hat{\mathbf{x}} + \underbrace{\begin{bmatrix} A & 0 \\ 0 & -1 \end{bmatrix}}_{\hat{\mathbf{B}}} \mathbf{u},$$

$$\underbrace{\begin{bmatrix} Q_a \\ F_d \end{bmatrix}}_{\hat{\mathbf{y}}} = \underbrace{\begin{bmatrix} A & 0 \\ 0 & 1 \end{bmatrix}}_{\hat{\mathbf{C}}} \hat{\mathbf{x}} + \underbrace{\begin{bmatrix} 0 & 0 \\ 0 & 0 \end{bmatrix}}_{\hat{\mathbf{D}}} \mathbf{u}, \quad (\text{S12})$$

where the new system matrices $\hat{\mathbf{L}}$, $\hat{\mathbf{A}}$, and $\hat{\mathbf{B}}$ are computed as described in (19).

The utility of congruent state-space transformations within the POG technique becomes evident when considering model reduction.

Comparison With Other Graphical Modeling Techniques

Figure S10 shows the dynamic modeling of the DC motor driving an hydraulic pump of Figure S1 using the three main graphical modeling techniques available in the literature: POG in Figure S10(a), BG in Figure S10(b), and EMR in Figure S10(c).

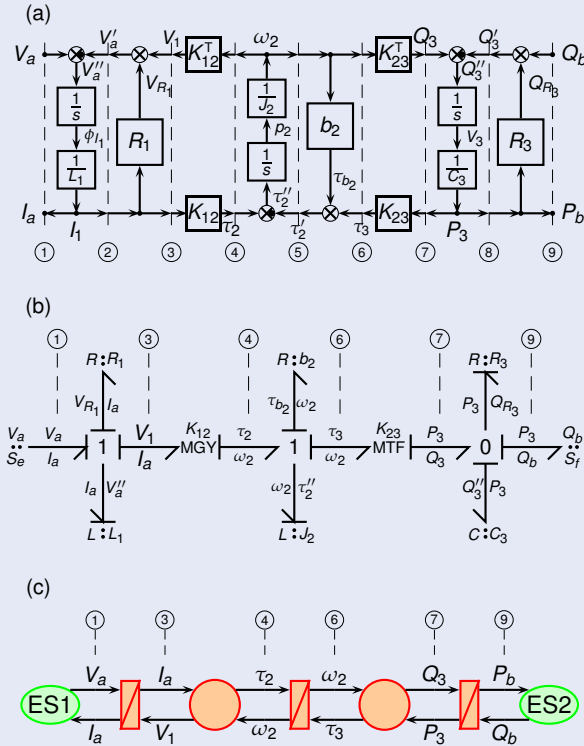


FIGURE S10 Different graphical modeling techniques available in the literature applied to model the DC motor driving an hydraulic pump of Figure S1. (a) Power-Oriented Graphs (POG) block scheme. (b) Bond Graph (BG) of the system. (c) Energetic Macroscopic Representation (EMR) of the system.

The main characteristics of POG, BG and EMR are compared in Table S1. The three graphical modeling techniques have different properties and characteristics that make them suitable for different objectives, as indicated in the last row of Table S1. The main advantages provided by POG over BG and EMR include: a) the symbolism, which is composed of standard blocks that can be found in standard Simulink libraries. b) the capability to derive the POG state-space model directly from the graphical description. The POG state-space model has a well defined energetic meaning, as described in the Section “POG

State-Space Model”, and enables the application of congruent state-space transformations which are particularly suitable for model reduction, as described in the Section “Congruent State-Space Transformations and Model Reduction”. c) the ease of use for non-expert users, thanks to a more intuitive graphical description which does not require the users to learn new specific graphical symbols. Furthermore, the POG schemes can be directly implemented in the Matlab/Simulink environment for direct simulation of the systems.

TABLE S1 A point-by-point comparison between the properties of the three main graphical modeling techniques available in the literature for modeling physical systems: Power-Oriented Graphs (POG), Bond Graph (BG), and Energetic Macroscopic Representation (EMR).

Property	POG	BG	EMR
Author - Year	R. Zanasi - 1991 [5]	H. M. Paynter - 1959 [3]	A. Bouscayrol - 2000 [8]
Extended Name	Power-Oriented Graphs	Bond Graph	Energetic Macroscopic Representation
Symbolism	Gains, Integrators and Summation Nodes	Arrows and Junctions	Energy domain-dependent Pictograms
Causality	Preferably integral	Preferably integral	Exclusively integral
Power Variables Direction Visibility	Yes	No	Yes
POG State-Space Model	Directly Obtainable from Graphical Description	Not Directly Obtainable from Graphical Description	Not Directly Obtainable from Graphical Description
Simulink Implementation	Use of Basic Blocks from Standard Libraries	Need of Dedicated Blocks	Need of Dedicated Blocks
Ease of Use for Non-Expert Users	More Intuitive	Less Intuitive	Average
Main Scope	Simulation and Analysis	Simulation and Design	Simulation and Control

THE POG TECHNIQUE: GENERAL RULES

In this section, a few general POG modeling rules are formally given with reference to an electrical circuit case study, whose Simscape schematic is shown in Figure 21(a).

Rule 1: The positive directions of the power variables v_e and v_f of all the PEs in the considered system must be chosen such that the power $P = v_e v_f$ is positive when entering the considered PE, see Figure 4(a).

Rule 2: The power variables v_e of all the PEs connected in parallel and the power variables v_f of all the PEs connected in series must share the same positive direction. In the example of Figure 21(a), this implies that the positive direction of current I_3 must be the same for both inductor L_3 and for resistor R_3 .

Rule 3: The dynamic PEs D_e and D_f in a POG block scheme must always be modeled guaranteeing integral causality [5], [6]. This implies that across elements D_e connected in parallel, such as capacitor C_4 in Figure 21(a), only admit the Elaboration Block (EB) configuration shown in Figure 15(a), as detailed in Figure 16(B) and Figure 16(e) for the capacitor C_4 . At the same time, through elements D_f connected in series, such as inductor L_3 in Figure 21(a), only admit the EB configuration shown in Figure 14(a), as detailed in Figure 16(A) and Figure 16(a) for the inductor L_3 . This rule comes from the application of Properties 1 and 2.

Rule 4: Static elements R admit all possible EB configurations in Figure 14 and in Figure 15. This rule comes from the application of Property 3.

Rule 5: If the considered physical system is stable, then all the loops of the corresponding POG block scheme must contain an odd number of minus signs. This rule comes from the fact that the series and parallel connections between physical elements can only be made using the EBs of the type reported in Figure 14 and in Figure 15.

STEP-BY-STEP MODELING OF PHYSICAL SYSTEMS

In this section, a step-by-step modeling procedure called Fast Modeling Power Oriented Graphs (FMPOG) is presented. The Fast Modeling POG is a guided, step-by-step procedure, based on the POG technique. It allows the transformation of physical system schematics into the corresponding POG block schemes and, ultimately, into the state-space models of the considered physical systems. In order to present the procedure, reference is made to the electrical circuit shown in Figure 21(a).

Step 1: Choose the positive directions of the state and input variables of the considered physical system. For the system in Figure 21(a), the input variables are the voltages V_a and V_b , while the state variables are the output power variables of all the system dynamic elements: the currents I_2 , I_3 and the voltages V_1 , V_4 . The chosen positive direction for each variable is highlighted by the corresponding arrow placed next to each variable, as denoted by \rightarrow and \uparrow in

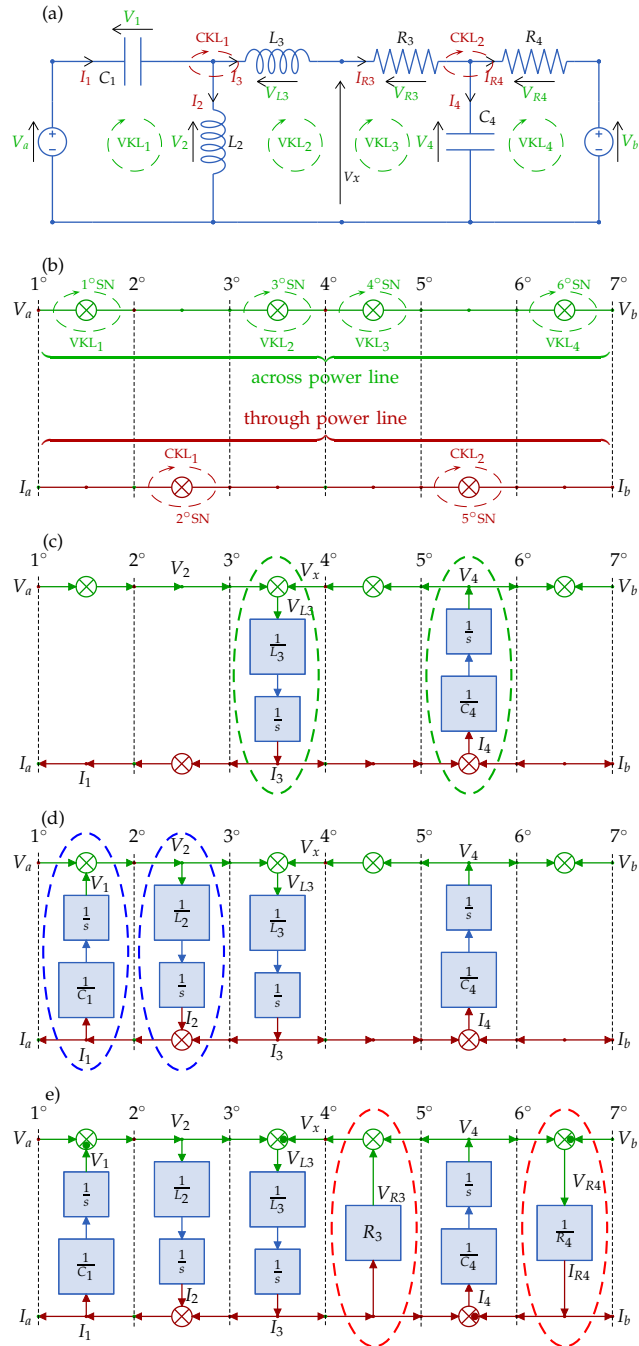


FIGURE 21 Electrical circuit taken as a case study. a) Simscape schematic, including the definition of the positive direction of the input and state variables representing Step 1 of the modeling procedure. b) Step 2 of the modeling procedure. c) Step 3 of the modeling procedure. d) Step 4 of the modeling procedure. e) Step 5 and Step 6 of the modeling procedure, resulting in the final POG block scheme of the system.

Figure 21(a). Since the power variable $I_3 = I_{R3}$ is in common to both elements L_3 and R_3 , it has the same positive direction for both the elements according to **Rule 2**.

Step 2: Choose the “across power line” and the “through power

line" and draw the series/parallel structure of the POG block scheme: draw a summation node on the **across power line** if the considered PE is connected in series and draw a summation node on the **through power line** if the considered PE is connected in parallel. In this case, the **across power line** and the **through power line** have been chosen to be the upper and the lower ones, respectively, as shown in Figure 21(b). By comparing the connections in Figure 13 with those of the PEs in the system of Figure 21(a), it can be noticed that: a) PEs C_1 , L_3 , R_3 and R_4 are connected in series, therefore the corresponding summation nodes 1°SN , 3°SN , 4°SN and 6°SN have been added in the **across power line** as shown in Figure 21.b, implementing the generalized Voltage Kirchhoff's Laws VKL_1 , VKL_2 , VKL_3 and VKL_4 , respectively; b) PEs L_2 and C_4 are connected in parallel, therefore the corresponding summation nodes 2°SN and 5°SN have been added in the **through power line**, see Figure 21.b, implementing the generalized Current Kirchhoff's Laws CKL_1 and CKL_2 , respectively.

Step 3: Add all the EBs of the dynamic elements D_f and D_e that only admit one possible configuration to the POG block scheme. This can be directly done by making use of **Rule 3**, which derives directly from Property 1. Since L_3 is a through element D_f connected in series, the only EB configuration guaranteeing integral causality is the one in Figure 16(A), that is the one encircled in green between power sections 3° and 4° in Figure 21(c) introducing the transfer function $\frac{I_3(s)}{V_{L3}(s)} = \frac{1}{L_3s}$. At the same time, since C_4 is an across PE D_e connected in parallel, the only EB configuration guaranteeing integral causality is the one in Figure 16(B), that is the one encircled in green between power sections 5° and 6° in Figure 21(c) introducing the transfer function $\frac{V_4(s)}{I_4(s)} = \frac{1}{C_4s}$.

Step 4: Add all the EBs of the dynamic elements D_f and D_e that admit two possible configurations to the POG block scheme. Once again, this can be directly done by recalling **Rule 3** and making the following observations, which derives directly from Property 2. Since L_2 is a through PE D_f connected in parallel, both the EB configurations in Figure 17(A) and Figure 17(B) guarantee integral causality. However, since its EB must be connected to the EB of L_3 , the only matching EB for L_2 is the one in Figure 17(A), as shown by the EB encircled in blue between power sections 2° and 3° in Figure 21(d) introducing the transfer function $\frac{I_2(s)}{V_2(s)} = \frac{1}{L_2s}$. Since C_1 is an across PE D_e connected in series, both the EB configurations in Figure 17(C) and Figure 17(D) guarantee integral causality. However, since its EB must be connected to the EB of L_2 and with voltage generator V_a , the only matching EB for PE C_1 is the one in Figure 17(D), as shown by the EB encircled in blue between power sections 1° and 2° in Figure 21(d) introducing the transfer function $\frac{V_1(s)}{I_1(s)} = \frac{1}{C_1s}$.

Step 5: Add all the EBs of the static elements R to the POG block scheme. According to **Rule 4**, resulting from the application

of Property 3, static elements R admit all the three EB configurations in Figure 14 when connected in series and all the three EB configurations in Figure 15 when connected in parallel. However, since the element R_3 in Figure 21(a) is connected in series and its EB must be connected to the EBs of elements L_3 and C_4 , the only possible configuration is the one shown in Figure 17(C), as shown by the EB encircled in red between power sections 4° and 5° in Figure 21(e) introducing the static relation $V_{R3} = R_3 I_3$. At the same time, since the element R_4 in Figure 21(a) is connected in series and its EB must be connected to that of the PE C_4 and with voltage generator V_b , the only possible configuration is the one shown in Figure 14(a), as shown by the EB encircled in red between power sections 6° and 7° in Figure 21(d) introducing the static relation $I_{R4} = \frac{1}{R_4} V_{R4}$. **Step 6:** Add the correct signs to the summation nodes of the POG block scheme according to the positive directions defined at **Step 1**. From the positive directions chosen at **Step 1** and recalling **Rule 1**, it is possible to correctly determine the signs p_1 and p_2 of the input power variables u_1 and u_2 of each summation node in order to have its output power variable $y = \sum_{i=1}^2 p_i u_i$ correctly defined. For the considered system, as shown in Figure 21(e), the output variables y of the summation nodes are given by:

$$\begin{aligned} 1^\circ\text{SN} &\rightarrow V_2 = V_a - V_1, & 2^\circ\text{SN} &\rightarrow I_1 = I_2 + I_3, \\ 3^\circ\text{SN} &\rightarrow V_{L3} = V_2 - V_x, & 4^\circ\text{SN} &\rightarrow V_x = V_{R3} + V_4, \\ 5^\circ\text{SN} &\rightarrow I_4 = I_3 - I_{R4}, & 6^\circ\text{SN} &\rightarrow V_{R4} = V_4 - V_b. \end{aligned} \quad (20)$$

As an example, for what concerns the 1°SN , the output power variable y is voltage V_2 , whereas the input power variables u_1 and u_2 are voltages V_a and V_1 , as shown in Figure 21(d). Applying VKL_1 in Figure 21(a), with the signs defined at **Step 1**, yields $y = V_2 = u_1 - u_2 = V_a - V_1$ as in (20). By making similar considerations, the remaining relations in (20) can be obtained, characterizing all the summation nodes in the resulting final POG block scheme illustrated in Figure 21(e).

It can be proven that, by applying the described FM-POG procedure, the obtained POG block scheme is always unique if no algebraic loops affect the considered physical system.

Modeling Example in the Hydraulic Domain

Reference is made to the hydraulic system in Figure 22(a), composed of the PEs L_1 , R_1 , C_2 , R_2 , L_3 , R_5 , C_4 , R_4 in the hydraulic domain, see Table 1. This system can be straightforwardly modeled using the FMPOG step-by-step procedure described in Section "Step-By-Step Modeling of Physical Systems", and making similar observations as in the previous case study. The system input variables are the pressure P_a and the volume flow rate Q_b , while the system state variables are the volume flow rates Q_1 and Q_3 , and the pressures P_2 and P_4 . The positive directions

The Fast Modeling POG is a guided, step-by-step procedure, based on the POG technique. It allows the transformation of physical system schematics into the corresponding POG block schemes and, ultimately, into the state-space models of the considered physical systems.

of the state and input variables are determined following **Step 1**, as shown in Figure 22(a). As per **Step 2**, the **across power line** and the **through power line** have been chosen to be the upper and the lower ones, respectively, as shown in Figure 22(b). In this example, it is possible to note the presence of a series PE element which is given by the parallel two more PEs, that are resistor R_5 and inductor L_3 in Figure 22(a), which leads to the introduction of the Nested Structure present in Figure 22(c). As per **Step 3**, the EBs of the dynamic elements admitting one configuration only are added to the POG block scheme, as shown by the EBs highlighted in orange in Figure 22(c). Subsequently, the EBs of the dynamic elements admitting two configurations are added to the POG block scheme according to **Step 4**, as shown by the EBs highlighted in blue in Figure 22(d). The next **Step 5** consists in adding the EBs of the static elements, as shown by the EBs highlighted in red in Figure 22(e). The correct signs are finally added to the summation nodes as described in **Step 6** resulting in the final POG block scheme of Figure 22(e). The Nested Structure highlighted in Figure 22(c) is characterized by the combination of the following **VKL** and **CKL**: $P_3 = P_2 - P_4$ and $Q_2' = Q_3 + Q_{R5}$.

DC Motor Supplying an Hydraulic Pump

The case study in Figure 23(a) involves three different energetic domains: electrical, mechanical and hydraulic. The input variables are the source voltage V_a of the DC motor and the volume flow rate Q_b , while the state variables are the current I_1 , the angular speed ω_2 and the pressure P_3 within the hydraulic capacitor C_3 . By applying the FMPOG step-by-step procedure illustrated in Section "Step-By-Step Modeling Of Physical Systems", the system in Figure 23(a) can be straightforwardly modeled following the intermediate steps shown in Figure 23(b)-(d). It is worth noticing that **Step 4** is not necessary in this case, since there are no dynamic PEs that admit two possible configurations in the considered system.

Remark 1

If one or more energy conversions take place within the system, the corresponding CBs need to be introduced into the POG scheme at **Step 2**, as shown in Figure 23(b), and

properly oriented after **Step 3** and **Step 4**, as shown in Figure 23(c)-(d). The presence of a CB of *gyrator* type causes the **across power line** and the **through power line** to swap places. The swap does not happen if the CB is of *transformer* type.

The system in Figure 23(a) exhibits two energy conversions, between the electrical/mechanical rotational domains and between the mechanical rotational/hydraulic domains. According to Remark 1, two CBs as that of Figure 7(d) are introduced in **Step 2**. The CBs are initially empty, as shown in Figure 23(b), and their orientation is to be determined as follows. By applying **Step 3**, the dynamic EBs shown in Figure 23(c) can be obtained, from which the proper orientation of the CBs can be determined according to the EBs next to them. The energy conversion coefficients K_{12} and K_{23} in the CBs of Figure 23(d) introduce the following relations:

$$\tau_2 = K_{12} I_1 \quad \text{and} \quad Q_3 = K_{23} \omega_2. \quad (21)$$

The **across** and **through** power lines swap places in correspondence of the second CB in Figure 23(d). This well agrees with what is stated in Remark 1, since the relation in (21) on the right physically describes a gyrator, that is the conversion of the across power variable ω_2 (angular speed) into the through power variable Q_3 (volume flow rate), as shown in Table 1.

SIMULATION COMPARISON AGAINST SIMSCAPE

This section shows a comparison between the simulation results provided by the Simscape schematic shown in Figure 21(a) and the simulation results provided by the obtained POG model shown in Figure 21(d), using the parameters, inputs, and initial conditions reported in Table 2. The obtained simulation results are reported in Figure 24: the very good superposition between the results provided by the Simscape and the POG dynamic models clearly show the correctness of the proposed FMPOG step-by-step procedure.

CONCLUSIONS

This article has proposed the Fast Modeling Power-Oriented Graphs (FMPOG), a step-by-step methodical procedure that

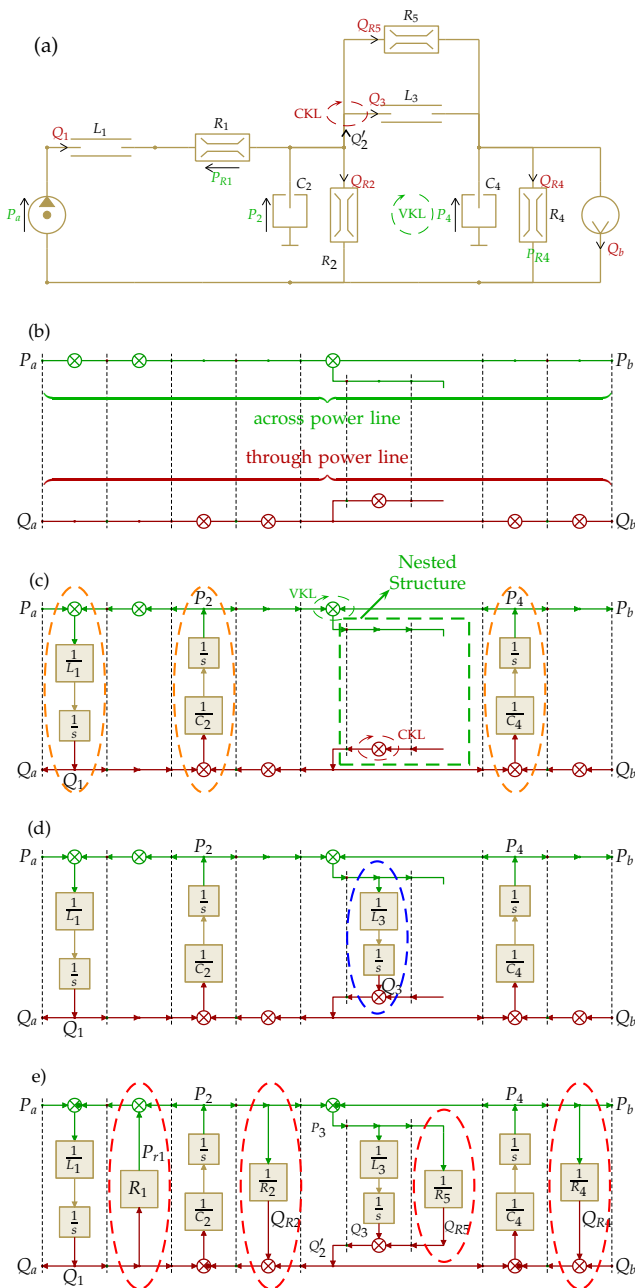


FIGURE 22 Hydraulic system taken as a second case study. a) Simscape schematic, including the definition of the positive direction of the input and state variables representing Step 1 of the modeling procedure. b) Step 2 of the modeling procedure. c) Step 3 of the modeling procedure. d) Step 4 of the modeling procedure. e) Step 5 and Step 6 of the modeling procedure, resulting in the final POG block scheme of the system.

guides the users through the derivation of the POG block schemes and, ultimately, the state-space models of physical systems starting from their schematics.

In order to present the FMPOG procedure, the first part of this article has been dedicated to the description of the fundamental principles and properties of the POG tech-

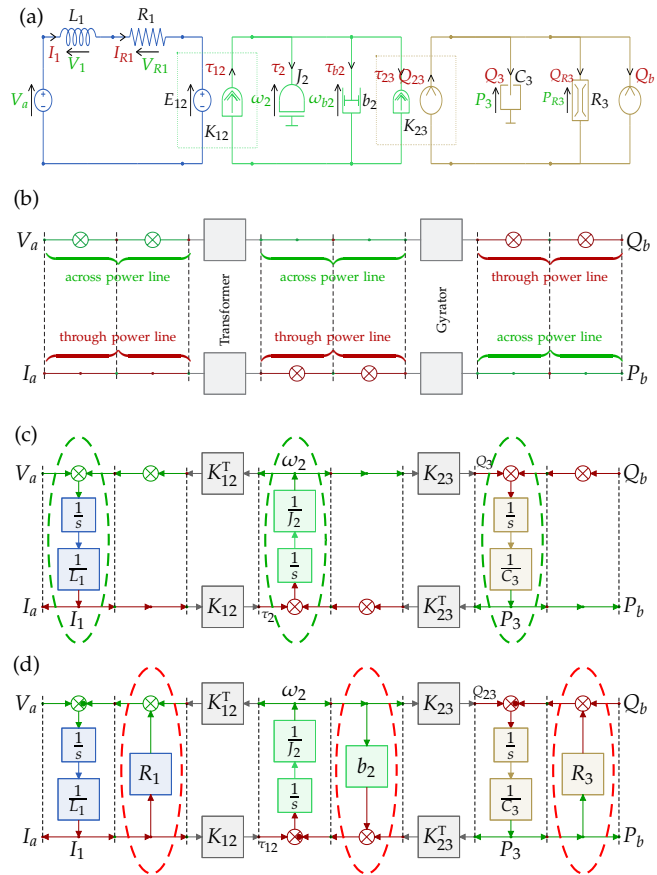


FIGURE 23 DC motor supplying an hydraulic pump taken as a third case study. a) Simscape schematic, including the definition of the positive direction of the input and state variables representing Step 1 of the modeling procedure. b) Step 2 of the modeling procedure. c) Step 3 of the modeling procedure, while Step 4 is not necessary for the considered system. d) Step 5 and Step 6 of the modeling procedure, resulting in the final POG block scheme of the system.

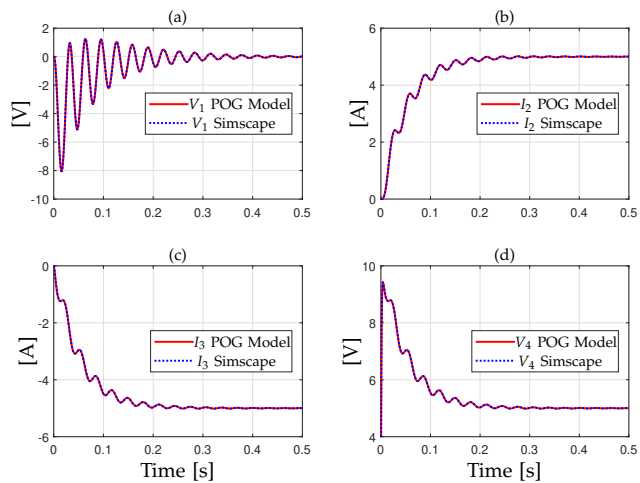


FIGURE 24 Comparison between the simulation results provided by the Simscape schematic of Figure 21(a) and the POG model of Figure 21(d). (a) The voltage V_1 . (b) The current I_2 . (c) The current I_3 . (d) The voltage V_4 .

TABLE 2 Simulation parameters, inputs and initial conditions for the simulation of the Simscape schematic of Figure 21(a) and of the POG model of Figure 21(d).

$V_a = 0$ [V], $V_b = 10$ [V]	$C_1 = C_4 = 1$ [mF]	$L_2 = L_3 = 50$ [mH]
$R_3 = R_4 = 1$ [Ω]	$V_{1_0} = V_{4_0} = 0$ [V]	$I_{2_0} = I_{3_0} = 0$ [A]

nique. The comparison of Power-Oriented Graphs with the two other main graphical modeling techniques in the literature, namely Bond Graph and Energetic Macroscopic Representation, has also been discussed. This has highlighted the convenient properties of the POG technique: its ease of use for non-expert users thanks to its user-friendly symbolism, which generates block schemes directly implementable in the Simulink environment, the capability to derive the state-space model directly from the POG block scheme, and its predisposition to model reduction through the use of congruent transformations. To help the readers to familiarize themselves with the POG technique, its application to various case studies of different complexity and in different energetic domains has also been addressed.

The proposed FMPOG procedure has the quality of being fully systematic and applicable to different physical systems in different energetic domains. Simulators allow the user to simulate the system schematic, but typically do not provide the user with the system dynamic model. On the other hand, the proposed FMPOG procedure allows for the direct reading of the system dynamic model from the POG block scheme, which is a functionality of great interest from a control point of view, in both graphical and analytical forms.

In order to demonstrate the versatility of the FMPOG procedure, we applied it to the modeling of three physical systems in the electrical, hydraulic, and electro-mechanical-hydraulic domains, respectively. We believe that the FMPOG procedure, developed within the framework of the POG modeling technique, is a powerful tool for engineers who need to quickly and automatically find the mathematical model of complex physical systems. In contrast, the derivation of these models may be more challenging and error-prone using standard, less systematic methods.

ACKNOWLEDGMENT

This work was partly supported by the University of Modena and Reggio Emilia through the action FARD (Finanziamento Ateneo Ricerca Dipartimentale) 2023/2024, and funded under the National Recovery and Resilience Plan (NRRP), Mission 04 Component 2 Investment 1.5 – NextGenerationEU, Call for tender n. 3277 dated 30/12/2021 Award Number: 0001052 dated 23/06/2022.

REFERENCES

- [1] J. C. Maxwell, "On physical lines of force," *Philosophical Magazine*, vol. 21, no. 139, pp. 161–175, March 1861.
- [2] G. Kron, *Tensor analysis of networks*. J. Wiley & Sons New York, 1939.
- [3] H. M. Paynter, "Analysis and design of engineering systems," MIT press, 1961.
- [4] P. J. Gawthrop and G. P. Bevan, "Bond-graph modeling," *IEEE Control Systems Magazine*, vol. 27, no. 2, pp. 24–45, 2007.
- [5] R. Zanasi, "Power-oriented modeling of dynamical systems for simulation," in *1991 IMACS Symposium on Modeling and Control of Technological Systems (MCTS)*, vol. 2, 1991, pp. 31–35.
- [6] —, "The power-oriented graphs technique: System modeling and basic properties," in *2010 IEEE Vehicle Power and Propulsion Conference*, 2010, pp. 1–6.
- [7] —, "Pog modeler: the web power-oriented graphs modeling program," *IFAC-PapersOnLine*, vol. 53, no. 2, pp. 13 030–13 035, 2020, 21st IFAC World Congress.
- [8] A. Bouscayrol, B. Davat, B. de Fornel, B. Francois, J. P. Hautier, F. Meibody-Tabar, and M. Pietrzak-David, "Multi-converter multi-machine systems: application for electromechanical drives," *The European Physical Journal - Applied Physics*, vol. 10, no. 2, p. 131–147, 2000.
- [9] A. Bouscayrol, B. Davat, B. de Fornel, B. Francois, J. Hautier, F. Meibody-Tabar, E. Monmasson, M. Pietrzak-David, H. Razik, E. Semail, and F. Benkhoris, "Control structures for multi-machine multi-converter systems with upstream coupling," *Mathematics and Computers in Simulation*, vol. 63, no. 3, pp. 261–270, 2003.
- [10] H. Yu, G. Lu, and Y. Zheng, "On the model-based networked control for singularly perturbed systems with nonlinear uncertainties," *Systems & Control Letters*, vol. 60, no. 9, pp. 739–746, 2011.
- [11] B. Bequette, *Process Control: Modeling, Design, and Simulation*. Upper Saddle River, NJ: Prentice Hall, 2003.
- [12] C. P. Pesce, "The Application of Lagrange Equations to Mechanical Systems With Mass Explicitly Dependent on Position," *Journal of Applied Mechanics*, vol. 70, no. 5, pp. 751–756, 10 2003.
- [13] C. Pesce, E. Tannuri, and L. Casetta, "The lagrange equations for systems with mass varying explicitly with position: some applications to offshore engineering," *Journal of The Brazilian Society of Mechanical Sciences and Engineering - J BRAZ SOC MECH SCI ENG*, vol. 28, no. 4, pp. 496–504, 12 2006.
- [14] C. Abdallah, D. Dawson, P. Dorato, and M. Jamshidi, "Survey of robust control for rigid robots," *IEEE Control Systems Magazine*, vol. 11, no. 2, pp. 24–30, 1991.
- [15] T. Lee, H. Lam, F. Leung, and P. Tam, "A practical fuzzy logic controller for the path tracking of wheeled mobile robots," *IEEE Control Systems Magazine*, vol. 23, no. 2, pp. 60–65, 2003.
- [16] Fuchs, Robert D., Hasuda, Yasuhiko, and James, Iain B., "Full toroidal ivt variator dynamics," in *SAE 2002 World Congress & Exhibition*. SAE International, mar 2002.
- [17] D. Tebaldi and R. Zanasi, "Systematic modeling of complex time-variant gear systems using a power-oriented approach," *Control Engineering Practice*, vol. 132, p. 105420, 2023.
- [18] M. Forstinger, R. Bauer, A. Hofer, and W. Rossegger, "Multivariable control of a test bed for differential gears," *Control Engineering Practice*, vol. 57, pp. 18–28, 2016.
- [19] H. L. Benford and M. B. Leising, "The lever analogy: A new tool in transmission analysis," *SAE Transactions*, vol. 90, no. 1, pp. 429–437, 1981.
- [20] D. Tebaldi and R. Zanasi, "Model-based cascade control of single-phase modular multilevel converters using ideal capacitor voltages reference," 2024. [Online]. Available: https://papers.ssrn.com/sol3/papers.cfm?abstract_id=4836302
- [21] D. Tebaldi, "Efficiency map-based pmsm parameters estimation using power-oriented modeling," *IEEE Access*, vol. 10, pp. 45954–45961, 2022.
- [22] N. Phankong, S. Manmai, K. Bhummittipich, and P. Nakawiwat, "Modeling of grid-connected with permanent magnet synchronous generator (pmsg) using voltage vector control," *Energy Procedia*, vol. 34, pp. 262–272, 2013.
- [23] G. Carli and S. S. Williamson, "Technical considerations on power conversion for electric and plug-in hybrid electric vehicle battery charging

- in photovoltaic installations," *IEEE Transactions on Power Electronics*, vol. 28, no. 12, pp. 5784–5792, 2013.
- [24] D. Zhou, K. Luo, Z. Shen, and J. Zou, "Deadbeat power distribution control of single-stage multiport inverter-fed pmsm drive for hybrid electric vehicles," *IEEE Transactions on Power Electronics*, vol. 38, no. 6, pp. 7586–7597, 2023.
- [25] L. Harnefors, A. Antonopoulos, S. Norrga, L. Angquist, and H.-P. Nee, "Dynamic analysis of modular multilevel converters," *IEEE Transactions on Industrial Electronics*, vol. 60, no. 7, pp. 2526–2537, 2013.
- [26] P.-B. Steckler, J.-Y. Gauthier, X. Lin-Shi, and F. Wallart, "Differential flatness-based, full-order nonlinear control of a modular multilevel converter (mmc)," *IEEE Transactions on Control Systems Technology*, vol. 30, no. 2, pp. 547–557, 2022.
- [27] L. Ben-Brahim, A. Gastli, M. Trabelsi, K. A. Ghazi, M. Houchati, and H. Abu-Rub, "Modular multilevel converter circulating current reduction using model predictive control," *IEEE Transactions on Industrial Electronics*, vol. 63, no. 6, pp. 3857–3866, 2016.
- [28] "Plecs documentation," last Accessed: June, 2024. [Online]. Available: <https://www.example.com/example-document>
- [29] H. K. Khalil, "High-gain observers in feedback control: Application to permanent magnet synchronous motors," *IEEE Control Systems Magazine*, vol. 37, no. 3, pp. 25–41, 2017.
- [30] R. Owen, M. Maggiore, and J. Apkarian, "A high-precision, magnetically levitated positioning stage: toward contactless actuation for industrial manufacturing," *IEEE Control Systems Magazine*, vol. 26, no. 3, pp. 82–95, 2006.
- [31] A. Tilli, A. Bosso, and C. Coniconi, "Towards sensorless observers for sinusoidal electric machines with variable speed and no mechanical model: A promising approach for pmsms," *Systems & Control Letters*, vol. 123, pp. 16–23, 2019.
- [32] H. Zhang, M. Dou, and J. Deng, "Loss-minimization strategy of nonsinusoidal back emf pmsm in multiple synchronous reference frames," *IEEE Transactions on Power Electronics*, vol. 35, no. 8, pp. 8335–8346, 2020.
- [33] J. Miller, "Hybrid electric vehicle propulsion system architectures of the e-cvt type," *IEEE Transactions on Power Electronics*, vol. 21, no. 3, pp. 756–767, 2006.
- [34] D. Tebaldi and R. Zanasi, "Modeling control and simulation of a power-split hybrid wheel loader," in *2021 29th Mediterranean Conference on Control and Automation (MED)*, 2021, pp. 465–471.
- [35] —, "A generalized procedure to model complex time-varying physical systems," in *2023 62nd IEEE Conference on Decision and Control (CDC)*, 2023, pp. 7721–7726.
- [36] Y. Liu, Y. Zhou, J. Wang, D. Qu, and F. Zhang, "Hydraulic system control for a hybrid continuously variable transmission based on an electric oil pump," *IEEE Transactions on Vehicular Technology*, vol. 67, no. 11, pp. 10398–10410, 2018.
- [37] J. De Baerdemaeker, A. Munack, H. Ramon, and H. Speckmann, "Mechatronic systems, communication, and control in precision agriculture," *IEEE Control Systems Magazine*, vol. 21, no. 5, pp. 48–70, 2001.
- [38] V. Kapila and S.-H. Lee, "Science and mechatronics-aided research for teachers," *IEEE Control Systems Magazine*, vol. 24, no. 5, pp. 24–30, 2004.
- [39] E. Garcia, M. A. Jimenez, P. G. De Santos, and M. Armada, "The evolution of robotics research," *IEEE Robotics & Automation Magazine*, vol. 14, no. 1, pp. 90–103, 2007.
- [40] R. V. Polyuga and A. J. van der Schaft, "Effort- and flow-constraint reduction methods for structure preserving model reduction of port-hamiltonian systems," *Systems & Control Letters*, vol. 61, no. 3, pp. 412–421, 2012.
- [41] G.-H. Geitner and G. Komurgoz, "Power flow modelling of dynamic systems - introduction to modern teaching tools," 2015. [Online]. Available: <https://arxiv.org/abs/1505.06828>
- [42] D. Jeltsema and J. M. Scherpen, "A power-based description of standard mechanical systems," *Systems & Control Letters*, vol. 56, no. 5, pp. 349–356, 2007.
- [43] D. Karnopp, "Power-conserving transformations: physical interpretations and applications using bond graphs," *Journal of the Franklin Institute*, vol. 288, no. 3, pp. 175–201, 1969.
- [44] D. M. Auslander, "Distributed System Simulation With Bilateral Delay-Line Models," *Journal of Basic Engineering*, vol. 90, no. 2, pp. 195–200, 06 1968.
- [45] R. C. Rosenberg, W. Feurzeig, and P. Wexelblat, "Bond graphs and enport in elementary physics instruction," *IEEE Transactions on Man-Machine Systems*, vol. 11, no. 4, pp. 170–174, 1970.
- [46] K. Sirivadha, E. F. Richards, and M. D. Anderson, "The application of bond graphs to electrical machinery and power engineering," *IEEE Transactions on Power Apparatus and Systems*, vol. PAS-102, no. 5, pp. 1176–1184, 1983.
- [47] H. Fraisse, J. Masson, F. Marthouret, and H. Morel, "Modeling of a non-linear conductive magnetic circuit. 2. bond graph formulation," *IEEE Transactions on Magnetics*, vol. 31, no. 6, pp. 4068–4070, 1995.
- [48] M. Kuang, M. Fodor, D. Hrovat, and M. Tran, "Hydraulic brake system modeling and control for active control of vehicle dynamics," in *Proceedings of the 1999 American Control Conference (Cat. No. 99CH36251)*, vol. 6, 1999, pp. 4538–4542 vol.6.
- [49] P. Borja, J. Ferguson, and A. van der Schaft, "Interconnection schemes in modeling and control," *IEEE Control Systems Letters*, vol. 7, pp. 2287–2292, 2023.
- [50] S. Benmoussa, B. O. Bouamama, and R. Merzouki, "Bond graph approach for plant fault detection and isolation: Application to intelligent autonomous vehicle," *IEEE Transactions on Automation Science and Engineering*, vol. 11, no. 2, pp. 585–593, 2014.
- [51] P. Kumar, I. Bensekrane, and R. Merzouki, "Power consumption modeling of wheeled mobile robots with multiple driving modes," *IEEE Transactions on Industrial Electronics*, vol. 70, no. 10, pp. 10282–10291, 2023.
- [52] P. J. Gawthrop, "Bond graph modeling of chemiosmotic biomolecular energy transduction," *IEEE Transactions on NanoBioscience*, vol. 16, no. 3, pp. 177–188, 2017.
- [53] D. Tebaldi and R. Zanasi, "Modeling control and simulation of a series hybrid propulsion system," in *2020 IEEE Vehicle Power and Propulsion Conference (VPPC)*, 2020, pp. 1–7.
- [54] K. Chen, P. Delarue, A. Bouscayrol, P.-E. Vidal, and M. Pietrzak-David, "Minimum copper loss and power distribution control strategies of double-inverter-fed wound-rotor induction machines using energetic macroscopic representation," *IEEE Transactions on Energy Conversion*, vol. 25, no. 3, pp. 642–651, 2010.
- [55] W. Lhomme, A. Bouscayrol, S. A. Syed, S. Roy, F. Gailly, and O. Pape, "Energy savings of a hybrid truck using a ravigneaux gear train," *IEEE Transactions on Vehicular Technology*, vol. 66, no. 10, pp. 8682–8692, 2017.
- [56] K. Li, W. Lhomme, and A. Bouscayrol, "A state of charge planning method of a plug-in hybrid electric truck with readily available navigation signals," *IEEE Transactions on Vehicular Technology*, vol. 73, no. 5, pp. 6093–6105, 2024.
- [57] "Descriptor state-space," last Accessed: May, 2024. [Online]. Available: <https://it.mathworks.com/help/simulink/slref/descriptorstatespace.html>

AUTHOR INFORMATION

Davide Tebaldi received the bachelor's degree in electronics engineering in 2015 and the master's degree in electronics engineering (cum laude) in 2018 from the University of Modena and Reggio Emilia, Italy. He received the Ph.D. degree in information and communication technologies in 2022 from the University of Modena and Reggio Emilia, discussing a thesis entitled Mathematical Modeling Control and Simulation of Hybrid Electric Vehicles. From October 2021 to January 2022, he was a visiting scholar at the Center for Automotive Research, The Ohio State University, Ohio, USA. From March 2022 to February 2023, he held a post-doc position at the University of Modena and Reggio Emilia. From March 2023, he has been an Assistant Professor at the University of Modena and Reggio Emilia. His research interests include the energetic modeling, control, energy efficiency analysis and simulation of mechatronic systems, with main application in the automotive, electrical machines and power electronics fields. Another branch of his research interests concerns the collaborative robotics field, with specific reference to the energy efficiency improvement and to the human-robot safe interaction.

Roberto Zanasi received the degree in electrical engineering (cum laude) from the University of Bologna in 1986. He received the Ph.D. degree in systems engineering in 1992. From 1994 to 1998, he was a Researcher in automatic controls with the Department of Electronics, Computer and System Science, University of Bologna. From 1998 to 2004, he was an Associate Professor of Automatic Control with the "Enzo Ferrari" Engineering Department, University of Modena and Reggio Emilia. From 2004, he has been a Full Professor of Automatic Control with the "Enzo Ferrari" Engineering Department, University of Modena and Reggio Emilia. He held the position of Visiting Scientist with the IRIMS of Moscow in 1991, at the MIT of Boston in 1992, and at the Université Catholique de Louvain in 1995. He has authored or coauthored many technical and scientific publications, and five books on automatic controls, simulation and digital control systems. His research interests include: mathematical modeling, power-oriented graphs, simulation, automotive, control of multiphase electrical motors, variable-structure systems, sliding mode control with integral action, robotics, linear and nonlinear control.

